Neutrino Flavor Conversions in Dense Media

by

Lei Ma

Supervisor:

Professor Huaiyu Duan

Doctor of Philosophy in Physics, University of New Mexico, 2018

Abstract

One of the interesting and important problems in astrophysics is the mechanism of core-collapse supernova explosions. Many numerical simulations have shown that the explosion shock would stall. Different proposals have been made to explain the core-collapse supernovae, among which the neutrino mechanism is promising and most researched one. To explore the mechanism, prediction of the neutrino flavors in core-collapse supernovae is crucial. Neutrino flavor conversions are altered by the matter, neutrinos themselves, as well as other factors such as the geometries of the neutrino emissions. The complexity of the problem requires breaking it down into investigations of each simple yet specific situation.

Neutrinos propagating through a matter background experience a potential which changes the flavor conversions. One of the important mechanisms is the Mikheyev–Smirnov–Wolfenstein effect. However, much more complicated density profiles of matter, such as periodic density profiles, may lead to large flavor conversion, which is dubbed as stimulated oscillations by J. Kneller et al. Mathematics of such large conversion has been established but without clear pictures. For the two-flavor scenario, neutrino oscillations is a two-level quantum system, and it reminds us of many two-level quantum problems that have been solved in the past. We draw analogies between neutrinos passing through matter and Rabi oscillations in optics, which allows us to calculate resonance conditions and flavor survival probability easily.

As for neutrinos flavors with high number densities, nonlinear interactions come into play since neutrino forward scattering provides another potential that is related to the flavor of the neutrinos themselves. Nonlinearity makes the flavor conversion hard to predict by intuition. The treatment is linearizing the equation of motion and identifying instabilities. One of the tricks in the realm is to utilize the dispersion relation. In principle, dispersion relations tell us how waves propagate for different wave numbers and frequencies. However, the neutrino problem is much more complicated. Situations that are inconsistent with the dispersion relation approach are identified.

Finally, forward scattering of supernova neutrinos are not the only thing that happens. During propagation around a supernova, neutrinos may be scattered in every direction, which forms a neutrino halo. The halo couples the neutrinos nonlocally, which then becomes a nonlocal boundary value problem. One of the solutions is the relaxation method. Starting from some state of neutrinos and relaxing the system into equilibrium has proven to be a working algorithm. A numerical algorithm is developed and neutrino line model with back scattering is investigated.

Chapter 1

Introduction

1.1 The Little Neutral One

The neutrino has been one of the most interesting particles that has ever been discovered. Its fanscinating history started with the observation of beta decay, i.e., the emission of electrons in nuclear decays, such as

$$_{6}^{14}\mathrm{C} \rightarrow {}_{7}^{17}\mathrm{N} + \mathrm{e}^- + \bar{\nu}_{\mathrm{e}}.$$
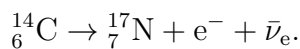
The fact that the electron energy spectrum in the beta decay process is continuous indicates the existence of a third product other than $_{7}^{17}\mathrm{N}$ and e^-. [Some History here!!!!!!!!!!!!!!!!!!!!!!!!!!!!!] It was then proven to be an anti-neutrino. In nuclear beta decays, the charged current weak interaction converts a down quark in the neutron to an up quark while releasing an electron and an anti-electron neutrino,

$$n \rightarrow p + e^- + \bar{\nu}_e. \tag{1.1}$$

More generally, the positron/electron emission and capture processes are all neutrino-related nuclear reactions which are listed in Table 1.1. There are three different flavors of neutrinos, namely the electron flavor, the muon flavor, and the tau flavor

as shown in Table 1.2. The first direct detection of neutrinos was done by Clyde Cowan and Frederick Reines in 1956 [1] who used nuclear reactor neutrinos as the source of the experiment.

Reaction Type	Process	Mediator(s)
Electron emission	${}^A_Z X \to {}^A_{Z+1} X' + e^- + \bar{\nu}_e$	$W^\pm$
Positron emission	${}^A_Z X \to {}^A_{Z-1} X' + e^+ + \nu_e$	$W^\pm$
Electron capture	${}^A_Z X + e^- \to {}^A_{Z-1} X' + \nu_e$	$W^\pm$
Positron capture	${}^A_Z X + e^+ \to {}^A_{Z+1} X' + \bar{\nu}_e$	$W^\pm$
$e^\pm$ annihilation	$e^- + e^+ \to \nu + \bar{\nu}$	$W^\pm, Z$
Bremsstrahlung	$X + X' \to X + X' + \nu + \bar{\nu}$	Z
$\nu(\bar{\nu})$ capture	${}^A_Z X + \overset{(-)}{\nu_e} \to {}^A_{Z\mp 1} X' + e^\pm$	$W^\pm$
$e^\pm \nu$ scattering	$e^- + \overset{(-)}{\nu} \to e^- + \overset{(-)}{\nu}$	$W^\pm, Z$
Nucleon scattering	${}^A_Z X + \overset{(-)}{\nu} \to {}^A_Z X + \overset{(-)}{\nu}$	Z

Table 1.1: Neutrino related nuclear and leptonic reactions.

[0.5ex] Electric Charge	0
Spin	1/2
Mass	< 2 eV
Interactions	Weak, Gravitation
Flavors	ν_e, ν_μ, ν_τ
Chirality	Left
Hypercharge	-1

Table 1.2: The physical properties of the neutrino [25].

1.2 Stellar Neutrinos

Besides man-made sources, neutrinos are also produced in many astrophysical environments.For example, numerous nuclear reactions occur in stellar cores which pro-
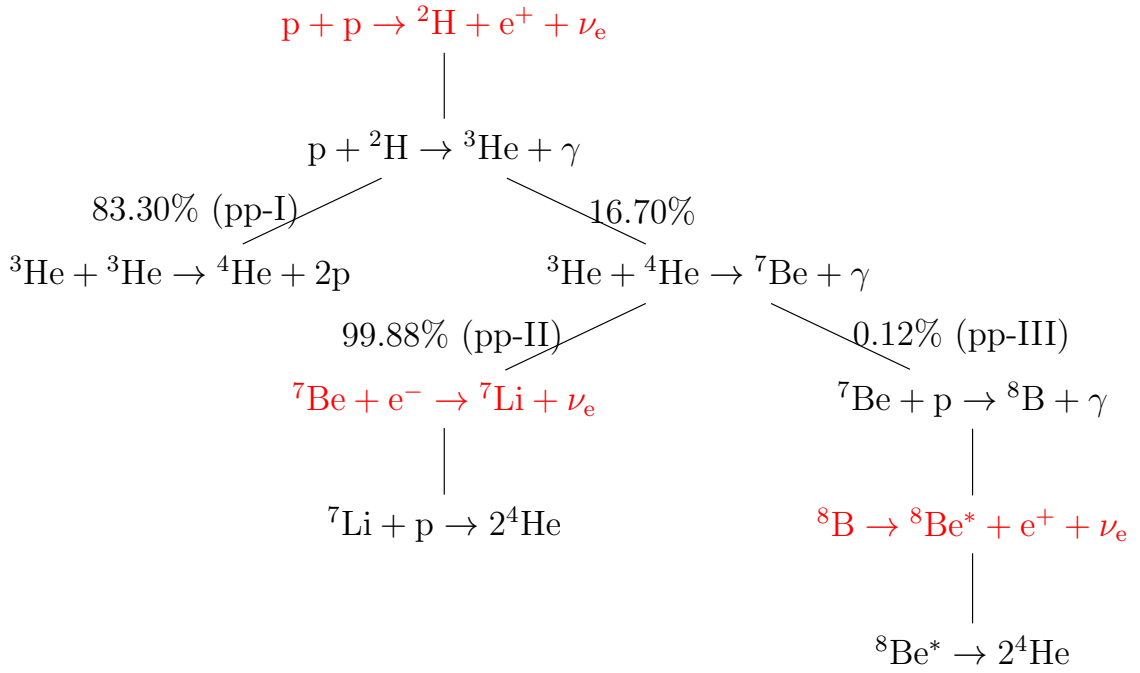
$$p + p \rightarrow {}^2H + e^+ + \nu_e$$

$$p + {}^2H \rightarrow {}^3He + \gamma$$

83.30% (pp-I)   16.70%

$${}^3He + {}^3He \rightarrow {}^4He + 2p$$ $${}^3He + {}^4He \rightarrow {}^7Be + \gamma$$

99.88% (pp-II)   0.12% (pp-III)

$${}^7Be + e^- \rightarrow {}^7Li + \nu_e$$ $${}^7Be + p \rightarrow {}^8B + \gamma$$

$${}^7Li + p \rightarrow 2{}^4He$$ $${}^8B \rightarrow {}^8Be^* + e^+ + \nu_e$$

$${}^8Be^* \rightarrow 2{}^4He$$

Figure 1.1: The pp chain reactions with the corresponding branching ratios. The branching ratios are taken from Ref. [9].

duce luminous neutrino fluxes. The most important nuclear reactions in the Sun are the pp chain reactions which are shown in Fig. 1.1. In order to calculate the neutrino spectrum we need the neutrino production rate in each reaction and the branching ratios. Solar neutrinos are mostly produced in the pp reaction, Be electron capture and B decay which are labeled in red in Fig 1.1:

$$p + p \rightarrow {}^2H + e^+ + \nu_e \qquad \leq 0.422\text{MeV},$$

$${}^7Be + e^- \rightarrow {}^7Li + \nu_e \qquad 0.862\text{MeV for } 90\%,$$

$$0.384\text{MeV for } 10\%,$$

$${}^8B \rightarrow {}^8Be^* + e^+ + \nu_e \qquad \leq 15\text{MeV}.$$

Even without the knowledge of the detailed reactions, the conservation of the electric charge and the electron lepton number will lead to the overall neutrino pro-

duction formula

$$4p + 2e^- \rightarrow {}^4He + 2\nu_e. \tag{1.2}$$

It is important to notice that two neutrinos are emitted for each α particle, i.e., ^{4}He, produced in the Sun. Using this simple relation, we can estimate the neutrino number flux emitted by the Sun. The energy released during the production of each α particle is the difference between the initial and final rest masses of the particles,

$$Q = 4m_p + 2m_e - m_\alpha = 26.7\text{MeV}, \tag{1.3}$$

where the mass of the neutrinos are neglected. On average, each neutrino carries away an energy of 0.2MeV and the rest of the energy is in the form of thermal energy $Q_\gamma = 26.3$MeV [19]. Since two neutrinos are emitted for the production of thermal energy Q_γ, the number flux of the solar neutrinos near the Earth is approximately

$$\Phi_\nu = \frac{2S_0}{Q_\gamma} \approx 6 \times 10^{10}\text{cm}^{-2}\text{s}^{-1}, \tag{1.4}$$

where the solar constant S_0 is the energy flux of solar photons on the top of the Eath atmosphere.

As the detection of neutrinos became feasible, Ray Davis and John Bahcall et al worked out the solar neutrino flux and led the Homestake experiment to measure the solar neutrinos. The results revealed that the neutrino flux detected was less than what was predicted by the standard solar model [3]. This is the solar neutrino problem. It is now known that the solution to the problem is related to the neutrino. The electron neutrinos produced in the solar core transform to other flavors while they travel to the Earth. This phonomenon is referred known as the flavor transformation of the neutrino, or neutrino oscillations. The theory of neutrino oscillations was first proposed by Pontecorvo in 1968 [2]. The field of neutrino oscillations has grown significantly into a broad field in physics since then.

1.3 Supernova Neutrinos

Another astronomical source of neutrinos is the core-collapse supernova explosion. Massive stars with masses larger than $6-8$ solar masses are very bright. However, violent delights have violent ends. When the core of a massive star runs out of nuclear fuel, it collapses under it's own gravity. During the collapse, the inner core is compressed to almost nuclear density, which has a stiff equation of state. The materials falling onto the highly compressed inner core are bounced outward which generates a shock wave and may lead to an explosion. However, supernova simulations to date show that the shock wave itself is not always energetic enough to produce the explosion [24]. In most cases, it stalls and becomes a standing accretion shock wave. To revive the shock, more energy has to be deposited behind the shock. A possible solution is to introduce reheating of the shock by neutrinos [24]. In fact 99% percent the energy released in a core-collapse supernova is carried away by neutrinos. In order to implement the neutrino-driven mechanism in computer simulations of supernovae, the flux and flavor content of the neutrinos have to be known everywhere behind the shock. Thus neutrino oscillations in dense matter become a key to the supernova explosion problem.

The average energy of the neutrinos $\langle E \rangle$ emitted during a supernova explosion is of the order of 10MeV [26], and the neutrino luminosity at the early epoch is approximately $10^{52} \text{ergs} \cdot \text{s}^{-1}$[CHANGE CITATIONSSSSSSSSSS!!!!!!!]. Therefore, the number density of the neutrinos at the radius R is

$$n \sim 10^{18} \text{cm}^{-3} \left(\frac{100\text{km}}{R} \right)^2 \left(\frac{10\text{MeV}}{\langle E \rangle} \right).$$

It turns out that the ambient dense neutrino medium has a significant impact on neutrino oscillations, which has been intensely investigated in the last decade [CITATION NEEDED].

Observation-wise, the neutrino signals from a galactic supernova can reveal a

great amount of information about the physical conditions inside the supernova. In fact, the detection of supernova neutrinos is on the task list of the Deep Underground Neutrino Experiment (DUNE) [27].

1.4 Organization of the Disseration

The rest of the disseration is organized as follows. In Chapter 2, I will review neutrino oscillations in vacuum and in environments with smooth matter density profiles. In Chapter 3, I will discuss my work on neutrino oscillations in oscillatory matter profiles, which can be decomposed into Fourier modes and interpreted as a superposition of Rabi oscillations. In Chapter **??**, I will first review how neutrino self-interactions can cause a dense neutrino medium to oscillate collectively. Then I will discuss my study on the dispersion relations of the collective modes of neutrino oscillations. I will also discuss a premilinary work on neutrino oscillations when both forward and backward neutrino fluxes are present. In Chapter **??**, I will summarize my work and discuss possible future directions of the field.

Chapter 2

General Principles of Neutrino Oscillations

Because the flavor eigenstates of the neutrino are not the same as its propagation eigenstates, it can change flavor while it propagates. In this chapter, I will use the two-flavor scheme to explain neutrino oscillations in some simple scenarios[1]. I will first discuss neutrino oscillations in vacuum. After explaining the general principles of neutrino oscillations in matter, I will show how the solar neutrino problem can be explained by neutrino oscillations. Finally, I will demonstrate the flavor isospin picture which can be used to visualize neutrino oscillations.

---

[1]In most physical problems, the two-flavor scheme is a good approximation to the phenomena of neutrino oscillations. The mass splits between the three mass eigenstates are so different that the corresponding oscillations occur on very different length scales. On the right length scale, the two-flavor scheme captures the prominent features of the neutrino oscillations of the corresponding mass split.

2.1   Vacuum Oscillations

Before working out the math, I can estimate the frequency of the oscillations of the neutrino between its flavors. In the natural units, frequency has the same dimension as energy (see Appendix **??**). Consider an electron neutrino with momentum p which is a superposition of the two mass eigenstates $|\nu_i\rangle$ $(i = 1, 2)$ with masses m_i, respectively. Since the neutrino masses are small, I can Taylor expand the energy of each mass eigenstate in terms of the corresponding mass:

$$\begin{aligned}
E_i &= \sqrt{m_i^2 + p^2} \\
&= p\sqrt{\frac{m_i^2}{p^2} + 1} \\
&\approx p + \frac{1}{2}\frac{m_i^2}{p}.
\end{aligned} \tag{2.1}$$

The first term in the above equation produces a global phase to the flavor wave function of the neutrino which does not affect neutrino flavor oscillations. The characteristic energy scale in the problem is the difference between the energies of the two mass eigenstates,

$$\omega_{\mathrm{v}} = \frac{m_2^2 - m_1^2}{2E} = \frac{\delta m^2}{2E}, \tag{2.2}$$

which turns out to be the vacuum oscillation frequency. Here $E = p$ is approximately the energy of the neutrino.

To work out the exact solution, I will utilize the Schrödinger equation. The wave function in flavor basis $\Psi^{(\mathrm{f})}$ is related to the wave function in mass basis $\Psi^{(\mathrm{v})}$ through a unitary mixing matrix U,

$$\Psi^{(\mathrm{f})} = \mathsf{U}\Psi^{(\mathrm{v})}, \tag{2.3}$$

where the upper indices $^{(\mathrm{v})}$ and $^{(\mathrm{f})}$ are used to denote the corresponding bases. The

mixing matrix can be expressed using the vacuum mixing angle θ_v,

$$\mathsf{U} = \begin{pmatrix} \cos\theta_v & \sin\theta_v \\ -\sin\theta_v & \cos\theta_v \end{pmatrix}. \tag{2.4}$$

In vacuum mass basis, the neutrino has a free propagation Hamiltonian

$$\mathsf{H}^{(v)} = \begin{pmatrix} E_1 & 0 \\ 0 & E_2 \end{pmatrix}. \tag{2.5}$$

To the first order, the Hamiltonian becomes

$$\mathsf{H}^{(v)} \approx \frac{1}{2E} \begin{pmatrix} m_1^2 & 0 \\ 0 & m_2^2 \end{pmatrix} + E\mathsf{I}$$

$$= \frac{1}{4E} \begin{pmatrix} -\delta m^2 & 0 \\ 0 & \delta m^2 \end{pmatrix} + \left(\frac{m_2^2 + m_1^2}{4E} + E \right) \mathsf{I}. \tag{2.6}$$

Because a multiple of the identity matrix I only gives an global phase to the neutrino flavor wave function, I will neglect it from now on, and the vacuum Hamiltonian simplifies to

$$\mathsf{H}^{(v)} = \frac{\delta m^2}{4E} \begin{pmatrix} -1 & 0 \\ 0 & 1 \end{pmatrix} = -\frac{\delta m^2}{4E}\sigma_3 = -\frac{\omega_v}{2}\sigma_3, \tag{2.7}$$

where

$$\sigma_1 = \begin{pmatrix} 0 & 1 \\ 1 & 0 \end{pmatrix}, \qquad \sigma_2 = \begin{pmatrix} 0 & -i \\ i & 0 \end{pmatrix}, \qquad \sigma_3 = \begin{pmatrix} 1 & 0 \\ 0 & -1 \end{pmatrix} \tag{2.8}$$

are the three Pauli matrices. The Schrödinger equation has the following simple solution in mass basis:

$$\Psi^{(v)}(t) = \begin{pmatrix} c_1(0)e^{i\omega_v t/2} \\ c_2(0)e^{-i\omega_v t/2} \end{pmatrix}. \tag{2.9}$$

Using Eqn. 2.3, I obtain the wave function in flavor basis,

$$\Psi^{(f)}(t) = \mathsf{U}\Psi^{(v)}(t) \tag{2.10}$$

$$= \begin{pmatrix} \cos\theta_v & \sin\theta_v \\ -\sin\theta_v & \cos\theta_v \end{pmatrix} \begin{pmatrix} c_1(0)e^{i\omega_v t/2} \\ c_2(0)e^{-i\omega_v t/2} \end{pmatrix}. \tag{2.11}$$

Alternatively, I can also determine the Hamiltonian in flavor basis first, which is

$$\mathsf{H}^{(f)} = \mathsf{U}\mathsf{H}^{(v)}\mathsf{U}^\dagger = -\frac{\omega_v}{2}\cos 2\theta_v \sigma_3 + \frac{\omega_v}{2}\sin 2\theta_v \sigma_1. \tag{2.12}$$

By solving the Schrödinger equation in flavor basis, I will obtain the same wave function as in Eqn. 2.11.

The probability for a neutrino emitted in the electron flavor at time $t = 0$ to be detected as the electron flavor at a later time t is

$$P(t) = 1 - \sin^2(2\theta_v)\sin^2\left(\frac{\omega_v t}{2}\right). \tag{2.13}$$

Since the neutrino travels with approximately the speed of light, the electron neutrino survival probability at a distance r from the source is

$$P(r) = 1 - \sin^2(2\theta_v)\sin^2\left(\frac{\omega_v}{2}r\right). \tag{2.14}$$

I plot the above result in Fig. 2.1 which clearly shows the oscillatory behavior. The oscillation length is determined by the characteristic energy scale ω_v, which confirms our qualitative method result in Eqn. 2.2. The oscillation amplitude is determined by $\sin^2(2\theta_v)$.

In nature, there are three neutrino flavors and, correspondingly, three neutrino mass eigenstates, which are shown in Fig. 2.2. Because there are two different characteristic energy scales, $\omega_{v,21} = \delta m_{21}^2/2E$ and $\omega_{v,32} = \delta m_{31}^2/2E$, two oscillation periods should occur, as shown in Fig. 2.3. The fast oscillations are determined by the larger energy scale, $\omega_{v,32}$, while the slow oscillations are determined by the smaller one $\omega_{v,21}$. For the inverted neutrino mass hierarchy (with $m_3 < m_1 < m_2$), the oscillation frequencies are the same as in the normal mass hierarchy (with $m_3 > m_2 > m_1$) since they have the same characteristic energy scales. However, they will develop different phases during oscillations.
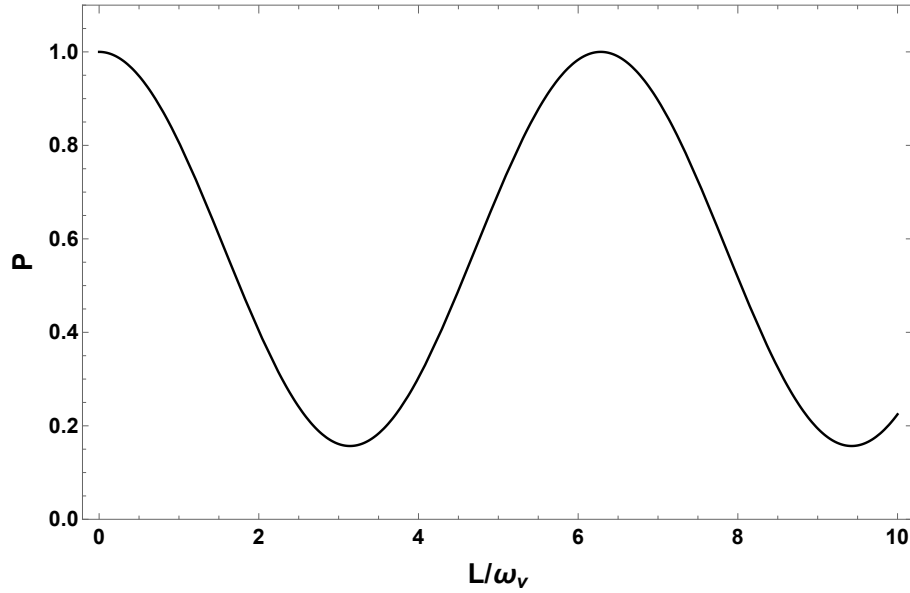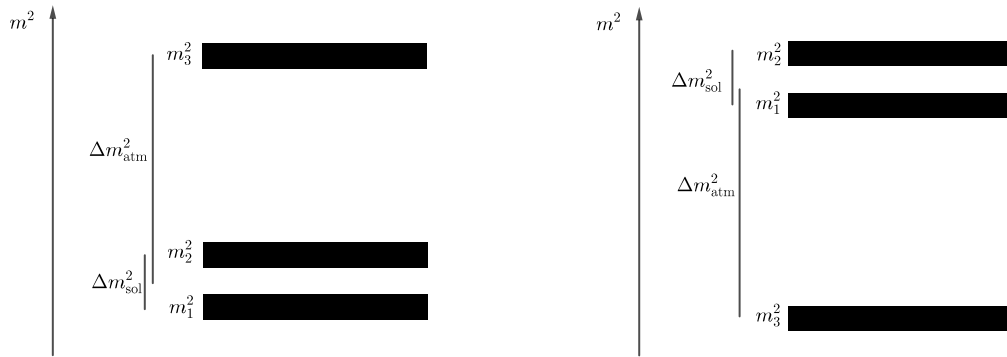
Figure 2.1: The electron flavor neutrino survival probability in vacuum oscillations as a function of distance r which is measured in terms of vacuum oscillation frequency ω_v. The mixing angle θ_v is given by $\sin^2\theta_\mathrm{v} = 0.30 \approx \sin^2\theta_{12}$.

(a) Normal hierarchy: the third mass is heavier than the first two.

(b) Inverted hierarchy: the third mass is smaller than the first two.

Figure 2.2: The order of the three neutrino masses. The difference between the first two masses is responsible for solar neutrino oscillations, and the difference between the third mass and the first two is responsible for atmospheric neutrino oscillations.
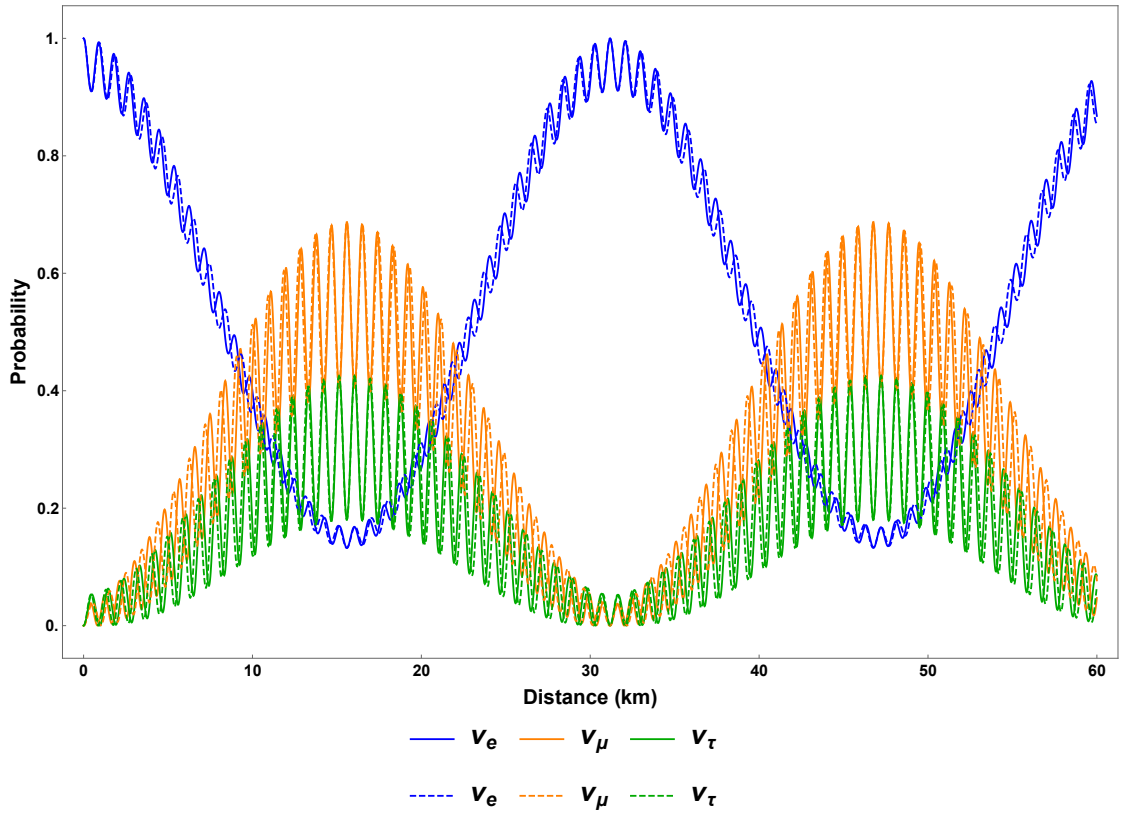
Figure 2.3: The probabilities for a 1MeV neutrino, which is in the electron flavor initially, in different flavors as functions of the distance in vacuum. The solid lines represent the normal hierarchy and the dashed lines represent the inverted hierarchy. The mixing angles are $\sin^2 \theta_{12} = 0.30$, $\sin^2 \theta_{13} = 0.023$, and $\sin^2 \theta_{23} = 0.41$, respectively, and the mass differences are $\delta m_{21}^2 = 7.9 \times 10^{-5} \text{eV}^2$ and $\delta m_{23}^2 = 2.7 \times 10^{-3} \text{eV}^2$.

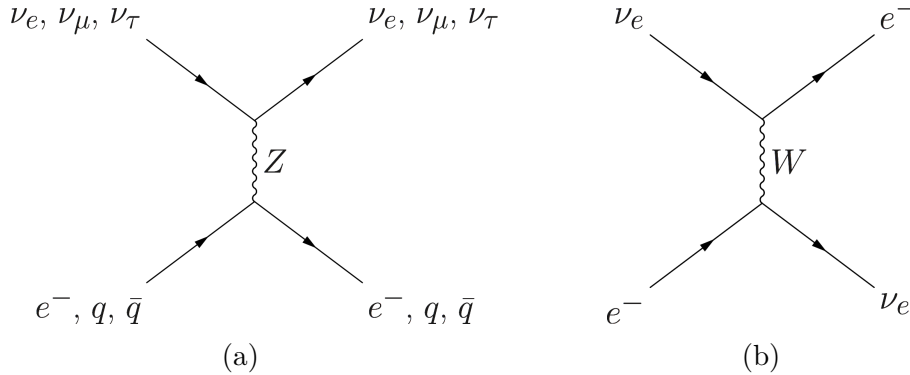## 2.2   Neutrino Oscillations in Matter

Figure 2.4: (a) The neutral current weak interaction does not distinguish between neutrino flavors and has no impact on neutrino oscillations. (b) The electron flavor neutrino acquires a unique refractive index contribution from the charged current weak interaction with ambient electrons.

In many astrophysical environments, such as stars and core-collapse supernovae, neutrinos are mostly produced at the center of the object and propagate through the dense matter envelope. Although this matter envelope is essentially transparent to neutrinos, the refractive indices of the neutrinos in matter are different than those in vacuum.[2] Because the neutral current weak interaction does not distinguish between neutrino flavors (see Fig. 2.4a), it has no impact on neutrino oscillations, and I will ignore it from now on. Meanwhile, the electrons and positrons in matter will cause electron flavor neutrinos to have refractive indices different than other neutrino flavors through the charged current weak interaction (see Fig. 2.4b). This leads to an effective potential

$$\mathsf{V}^{(\mathrm{f})} = \frac{\sqrt{2}G_{\mathrm{F}}n_{\mathrm{e}}}{2}\sigma_3, \tag{2.15}$$

where G_{F} is Fermi constant and n_{e} is net number density of the electron. As usual,

---

[2]The word "matter" in this disseration refers to ordinary matter composed of electrons, positrons, nucleons and nuclei. We assume that the temperature and density of the environment are not high enough to produce muons and tau particles. We will discuss the effect of dense neutrino medium in Chapter **??**.

I have ignored the trace terms in the above equation.

The Hamiltonian with the matter effect is the combination of Eqn. 2.12 and Eqn. 2.15:

$$\mathsf{H}^{(\text{f})} = \left(\frac{\lambda}{2} - \frac{\omega_\text{v}}{2} \cos 2\theta_\text{v} \right) \sigma_3 + \frac{\omega_\text{v}}{2} \sin 2\theta_\text{v} \sigma_1, \tag{2.16}$$

where

$$\lambda = \sqrt{2} G_\text{F} n_\text{e}. \tag{2.17}$$

Due to the off-diagonal terms in $\mathsf{H}^{(\text{f})}$, the neutrino will experience oscillations in flavor. A resonance with the maximum flavor mixing occurs when the diagonal terms of $\mathsf{H}^{(\text{f})}$ vanish,

$$\frac{\lambda}{2} - \frac{\omega}{2} \cos 2\theta_\text{v} = 0, \tag{2.18}$$

which gives the Mikheyev–Smirnov–Wolfenstein (MSW) resonance condition.

2.3   Neutrino Oscillations in the Sun

The neutrinos produced in the solar core experience decreasing matter density as they travel outward through the Sun. The neutrino propagation eigenstates are different from the flavor states in general [4]. Because the density change inside the Sun is not dramatic, the flavor quantum states of the neutrinos will evolve adiabatically inside the Sun.

The values of the instantaneous eigenstates of the Hamiltonian, known as the heavy and light states, are

$$\varepsilon_\text{H} = \frac{\omega_\text{v}}{2} \sqrt{\hat{\lambda} + 1 - 2\hat{\lambda} \cos 2\theta_\text{v}}, \tag{2.19}$$

$$\varepsilon_\text{L} = -\frac{\omega_\text{v}}{2} \sqrt{\hat{\lambda} + 1 - 2\hat{\lambda} \cos 2\theta_\text{v}}, \tag{2.20}$$
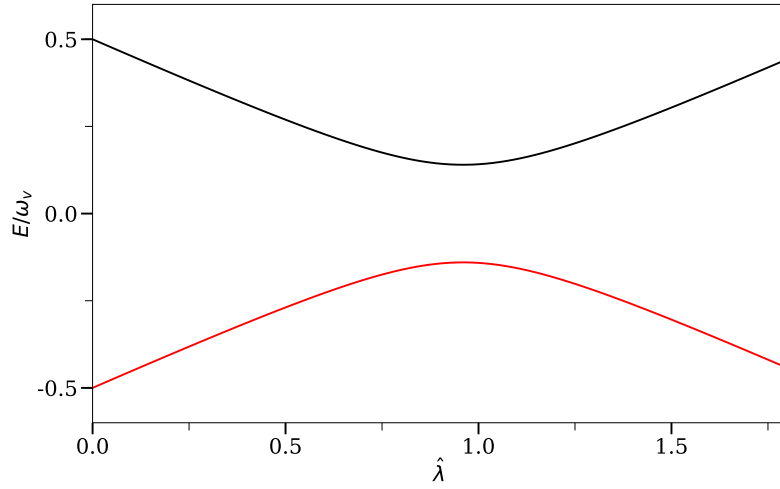
Figure 2.5: The two eigenvalues of the neutrino Hamiltonian as functions of matter potential $\hat{\lambda}$. I have used $\sin^2 \theta_v = 0.02 \approx \sin^2 \theta_{13}$.

where

$$\hat{\lambda} = \frac{\lambda}{\omega_v}. \tag{2.21}$$

In Fig. 2.5, I show the two eigenvalues of the neutrino Hamiltonian as functions of the matter potential $\hat{\lambda}$.

For a very high matter density, the heavy state of the neutrino $|\nu_H\rangle$ is almost the same as $|\nu_e\rangle$. As the matter density decreases, $|\nu_H\rangle$ becomes a mixture of different neutrino flavors. As the neutrino reaches the surface of the Sun, where the matter density is approximately zero, $|\nu_H\rangle$ is about the same as vacuum mass eigenstate $|\nu_2\rangle$. As a result, the electron flavor neutrinos produced at the solar core are partially converted to other flavors as they reach the surface of the Sun. This explains the solar neutrino problem.
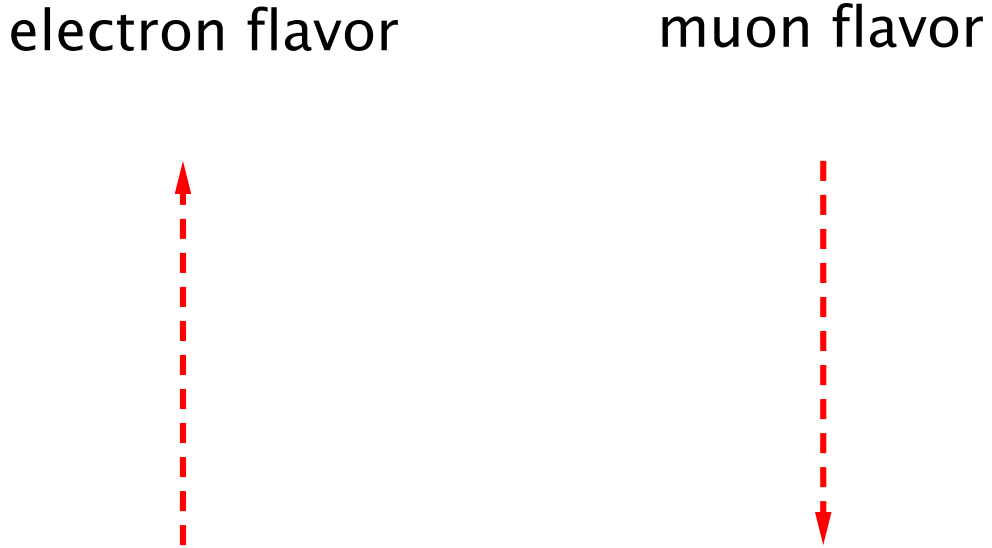
electron flavor   muon flavor

Figure 2.6: In the flavor isospin picture, a flavor isospin pointing upward, i.e., along the third axis in flavor space, indicates that the neutrino is in the electron flavor, while the downward direction indicates the other flavor, such as the muon flavor.

2.4   Flavor Isospin Formalism

The Hamiltonian for two-flavor neutrino oscillations describes a two-level quantum system. It is known that two-level quantum systems can be visualized using the Bloch sphere. In the realm of neutrino physics, the neutrino flavor isospin was introduced for such purpose [12].

Every two-by-two Hermitian matrix can be expanded in the quaternian basis. For example, the Hamiltonian for neutrino oscillations in vacuum (in flavor basis) can be written as

$$\mathsf{H}^{(\mathrm{f})} = -\frac{\vec{\sigma}}{2} \cdot \vec{H},\tag{2.22}$$

where

$$\vec{H} = \omega_{\mathrm{v}} \begin{pmatrix} \sin\theta_{\mathrm{v}} \\ 0 \\ \cos 2\theta_{\mathrm{v}} \end{pmatrix},$$

which is a vector of length ω_{v} and tilted away from the third axis by the angle $2\theta_{\mathrm{v}}$. Throughout the dissertation, I will use " $\vec{}$ " to denote a vector in flavor space. The flavor quantum state of the neutrino is represented by the flavor isospin, which is defined as

$$\vec{s} = \Psi^{(\mathrm{f})\dagger} \frac{\vec{\sigma}}{2} \Psi^{(\mathrm{f})}. \tag{2.23}$$

As shown in Fig. 2.6, the direction of the flavor isospin in flavor space shows the flavor content of the neutrino. A flavor isospin pointing upward in flavor space, i.e., along the direction of the third axis, denotes the electron flavor by definition. Correspondingly, the equation of motion for the flavor isospin describes its precession around the vector $\vec{H}$,

$$\dot{\vec{s}} = \vec{s} \times \vec{H}. \tag{2.24}$$

In the flavor isospin formalism, the electron flavor survival probability is

$$P = \frac{1}{2} + s_3,$$

where s_3 is the third component of the flavor isospin. Therefore, the precession of the flavor isospin corresponds to a periodic oscillation between the two neutrino flavors (see Fig. 2.7). The oscillation frequency is trivially read out from Eqn. 2.24,

$$\omega_{\mathrm{v}} = |\vec{H}|. \tag{2.25}$$

The MSW effect can also be easily explained using the flavor isospin picture. The
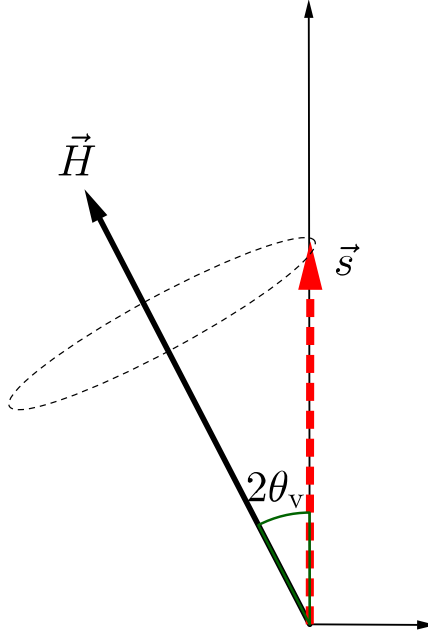
Figure 2.7: Vacuum oscillations in the flavor isospin picture. The flavor isospin of a neutrino starting with the electron flavor will precess around the static "Hamiltonian vector" $\vec{H}$, which gives a periodic flavor oscillation according to Eqn. 2.4.

Hamiltonian for the neutrino flavor evolution in the presence of dense matter is

$$\mathsf{H}^{(\mathrm{f})} = \frac{\omega_{\mathrm{v}}}{2}\left(-\cos 2\theta_{\mathrm{v}}\sigma_3 + \sin 2\theta_{\mathrm{v}}\sigma_1\right) + \frac{\lambda(x)}{2}\sigma_3$$

$$\Rightarrow \vec{H} = \vec{H}_{\mathrm{v}} + \vec{H}_{\mathrm{m}}(x) = \omega_{\mathrm{v}}\begin{pmatrix} -\sin 2\theta_{\mathrm{v}} \\ 0 \\ \cos 2\theta_{\mathrm{v}} \end{pmatrix} + \begin{pmatrix} 0 \\ 0 \\ -\lambda(x) \end{pmatrix},$$

where $\vec{H}_{\mathrm{v}}$ is the vacuum contribution, and $\vec{H}_{\mathrm{m}}(x)$ is the matter potential contribution. The precession motion of the flavor isospin of the neutrino in the presence of dense matter is visualized in Fig. 2.8. The MSW resonance condition in Eqn. 2.18 corresponds to the senario that the overall "Hamiltonian vector" $\vec{H}$ is perpendicular to the third axis in flavor space. In this case, the flavor isospin rotates in the plane spanned by the second and third axes which gives maxium flavor oscillations
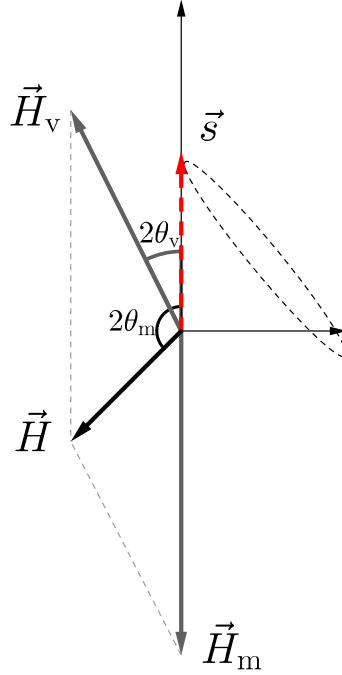
Figure 2.8: Neutrino oscillations in flavor isospin picture, with the presence of matter potential. The flavor isospin is denoted as red dashed arrow. It starts from electron flavor. The two gray vectors stand for the Hamiltonians of vacuum $\vec{H}_\mathrm{v}$ and matter $\vec{H}_\mathrm{m}$.

(see Fig. 2.9).

The adiabatic flavor evolution of the neutrino in varying matter density that was discussed in Sec. 2.3 can also be easily understood by the flavor-isospin picture. In the region where the matter density is high, the total "Hamiltonian vector" $\vec{H}$ points downward. Therefore, a neutrino produced in the electron flavor will experience very little oscillations because its flavor isospin $\vec{s}$ is almost anti-parallel to $\vec{H}$ (see Fig. 2.10a). If the matter density along the propagation trajectory of the neutrino decreases slowly, the $\vec{s}$ will stay anti-parallel to $\vec{H}$ as $\vec{H}$ rotates (see Fig. 2.10b). When the neutrino reaches the region with very low matter density, its flavor isospin becomes anti-parallel to $\vec{H}_\mathrm{v}$, which implies that the neutrino is in $|\nu_2\rangle$ (see Fig. 2.10).
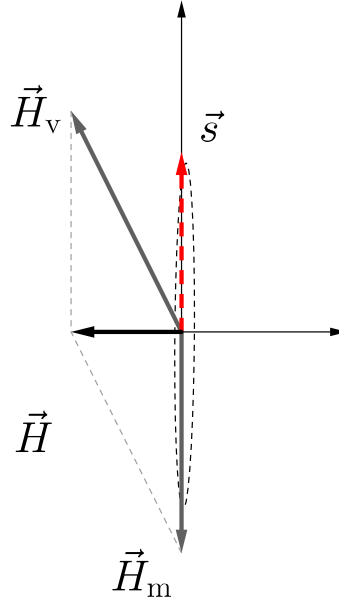
Figure 2.9: MSW resonance happens when electron neutrinos go through a critical matter density.

2.5 Summary

Neutrino oscillations in vacuum and in matter with a smooth profile have been explained. The neutrino oscillations phenomena reveals a secret of the nature of the neutrino, i.e., its flavor states are not the same as the propagation eigenstates of the Hamiltonian. As a result, a neutrino produced in the pure flavor state through weak interaction will not remain in the same flavor state as it propagates, but oscillate between different flavors. The problem of neutrino oscillations in an environment with rapidly varying matter densities is significant more difficult than that in a smooth profile. This will be discussed in the next chapter.
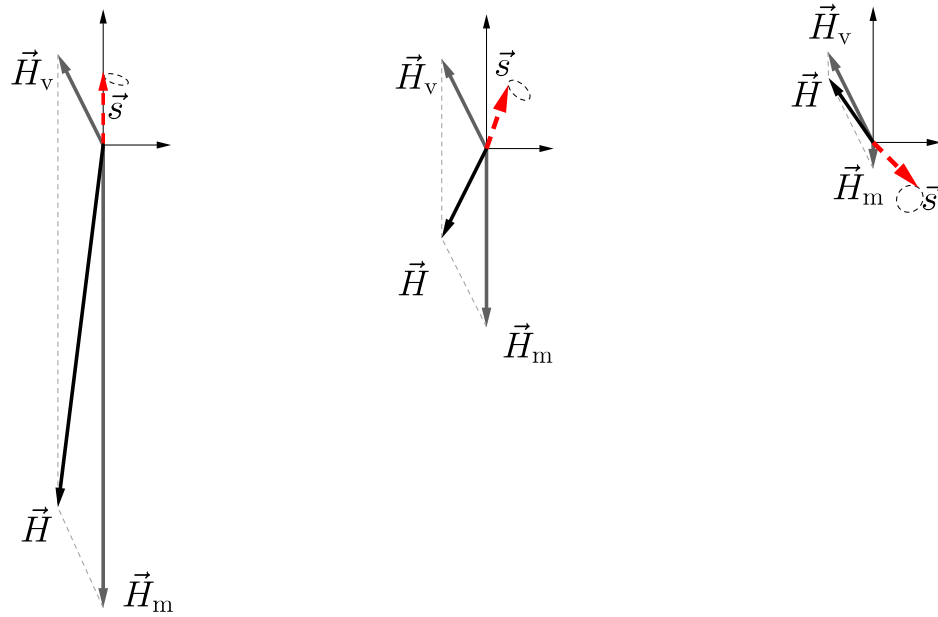
(a) High matter density   (b) Medium matter density   (c) Low matter density

Figure 2.10: Flavor isospin picture of neutrino oscillations in matter. $\vec{H}_{\mathrm{v}}$ is the vacuum contribution to Hamiltonian, and $\vec{H}_{\mathrm{m}}$ corresponds to the matter potential.

Chapter 3

Neutrino Oscillations in Oscillatory Matter Profile

In certain regions inside a star or a supernova where convection is prominent, the matter density varies rapidly as a function of distance [23, 22]. The neutrino flavor evolution in such environments is qualitatively different than that in a smooth density profile [5, 6, 8, 14, 18, 20, 21]. For example, the flavor conversion of the neutrino is greatly enhanced if the matter density fluctuates with certain wave numbers. This is known as parametric resonance.

To understand this interesting phenonema I will first introduce the background matter basis where the equation of motion simplifies. After demonstrating the simplest example of the parametric resonance in the presence of a sinusoidal matter profile with the Rabi formula, I will explain the interference effect when there exist multiple Fourier modes in the matter profile. Then I will show how to use the Jacobi-Anger expansion to decompose an arbitrary matter profile into a infinite sum of Fourier modes and how to apply the Rabi formula in these scenarios.

In Sec. 3.5 we discuss the technique of decomposing the neutrino flavor conver-

sions into summation of Rabi oscillations, by applying a specific unitary transformation and the Jacobi-Anger expansion. As the system is exactly decomposed into multiple Rabi oscillations, we can interpret neutrino flavor oscillations in any matter density fluctuations, in principle. As an example, we solve the neutrino flavor transitions in a castle wall matter profile, which contains infinite frequencies from the aspect of Fourier series. Finally I will discuss an algorithm to select the Fourier modes of a matter profile that have the largest impact on the flavor conversion of the neutrino.

3.1 Background Matter Basis

For a uniform matter density $\lambda(r) = \lambda_0$, one can define a matter basis in which the Hamiltonian is diagonalized:

$$\mathsf{H}^{(\mathrm{m})} = \mathsf{U}^\dagger \mathsf{H}^{(\mathrm{f})} \mathsf{U} = -\frac{\omega_\mathrm{m}}{2}\sigma_3, \tag{3.1}$$

where

$$\mathsf{U} = \begin{pmatrix} \cos\theta_\mathrm{m} & \sin\theta_\mathrm{m} \\ \sin\theta_\mathrm{m} & \cos\theta_\mathrm{m} \end{pmatrix} \tag{3.2}$$

with

$$\theta_\mathrm{m} = \frac{1}{2}\arctan\left(\frac{\sin 2\theta_\mathrm{v}}{\cos 2\theta_\mathrm{v} - \lambda_0/\omega_\mathrm{v}}\right),$$

and

$$\omega_\mathrm{m} = \omega_\mathrm{v}\sqrt{(\lambda_0/\omega_\mathrm{v} - \cos(2\theta_\mathrm{v}))^2 + \sin^2(2\theta_\mathrm{v})} \tag{3.3}$$

is the neutrino oscillations frequency in matter.

In the rest of the chaper, I will consider profiles of the form

$$\lambda(r) = \lambda_0 + \delta\lambda(r), \tag{3.4}$$

where $\delta\lambda(r)$ describes the fluctuation of the matter density. I will use the background matter basis defined by Eqn. 3.1 and Eqn. 3.3. In this basis, the Hamiltonian reads

$$\mathsf{H}^{(\mathrm{m})} = -\frac{\omega_{\mathrm{m}}}{2}\sigma_3 + \frac{1}{2}\delta\lambda(r)\cos 2\theta_{\mathrm{m}}\sigma_3 - \frac{1}{2}\delta\lambda(r)\sin 2\theta_{\mathrm{m}}\sigma_1. \tag{3.5}$$

In the background matter basis, the wave function describes the amplitudes of different eigenstates defined when there is only background matter density λ_0. Given the transition probability between the these eigenstates, it is trivial to calculate the flavor conversion. Since I'll concentrate on the flavor conversion due to the matter fluctuations, I'll only discuss the transition between mass states in the background matter basis.

All the numerical examples in this chapter are calculated with $\sin^2(2\theta_{\mathrm{v}}) = 0.093$ and $\omega_{\mathrm{v}} = 3.75 \times 10^{-17}\mathrm{MeV}^2$.

3.2 Single Frequency Matter Profile and Rabi oscillations

In this section I will present a simple picture to explain neutrino parametric resonance in matter by utilizing the theory of Rabi oscillations. Rabi oscillations have been well studied in quantum optics [16]. It describes the transition between different quantum states due to an oscillatory external driving field, where maximum transition or resonance happens when the frequency of external driving field equals the energy gap. In this section, I will first derive the Rabi oscillation transition probabilities using neutrino flavor isospin method introduced in Ref. [13]. Then I will apply the results of Rabi oscillations to neutrino oscillations in single frequency matter profile.

$$\varepsilon_2 = \frac{\omega_{\mathrm{R}}}{2}$$ _____

incoming light

with frequency ω

$$\varepsilon_1 = -\frac{\omega_{\mathrm{R}}}{2}$$ _____

Figure 3.1: Schematic illustration of Rabi oscillations system. The two level system has two energy states at $\varepsilon_1 = -\frac{\omega_{\mathrm{R}}}{2}$ and $\varepsilon_2 = \frac{\omega_{\mathrm{R}}}{2}$. Resonance happens when the freuquency of the driving field ω equals the energy gap ω_{R}, i.e., $\omega = \omega_{\mathrm{R}}$.

3.2.1 Rabi Oscillations

An example of Rabi oscillations is a two-level quantum system with energy gap $\delta\varepsilon = \omega_{\mathrm{R}}$ and light of frequency ω shining on the two-level system (see Fig. 3.1). The Hamiltonian for Rabi oscillation is

$$\mathsf{H}_{\mathrm{R}} = -\frac{\omega_{\mathrm{R}}}{2}\sigma_3 - \frac{A_{\mathrm{R}}}{2}\left(\cos(k_{\mathrm{R}}t + \phi_{\mathrm{R}})\sigma_1 - \sin(k_{\mathrm{R}}t + \phi_{\mathrm{R}})\sigma_2\right), \tag{3.6}$$

in which ω_{R} serves as the energy split of the two level system, while A_{R} and k_{R} are the strength and frequency of the driving field, respectively. The Hamiltonian H_{R} can be mapped into a vector using the flavor isospin picture:

$$\vec{H}_{\mathrm{R}} = \vec{H}_3 + \vec{H}_+,$$

where

$$\vec{H}_3 = \begin{pmatrix} 0 \\ 0 \\ \omega_{\mathrm{R}} \end{pmatrix}, \tag{3.7}$$

$$\vec{H}_+ = \begin{pmatrix} A_{\mathrm{R}}\cos(k_{\mathrm{R}}t + \phi_{\mathrm{R}}) \\ -A_{\mathrm{R}}\sin(k_{\mathrm{R}}t + \phi_{\mathrm{R}}) \\ 0 \end{pmatrix}. \tag{3.8}$$

The above two vectors are mapped into a Cartesian coordinate system similar to the flavor isospin space [1]. The vector $\vec{H}_3$ is the vector aligned with the third axis, $\vec{H}_+$ is a rotating vectors in a plane perpendicular to $\vec{H}_3$ (see Fig. 3.2a). The wave function $\Psi = (\psi_1, \psi_2)^{\mathrm{T}}$ is also used to define the state vector $\vec{s}$

$$\vec{s} = \Psi^\dagger \frac{\vec{\sigma}}{2} \Psi \tag{3.9}$$

$$= \frac{1}{2} \begin{pmatrix} 2\,\mathrm{Re}\,(\psi_1^*\psi_2) \\ 2\,\mathrm{Im}\,(\psi_1^*\psi_2) \\ |\psi_1|^2 - |\psi_2|^2 \end{pmatrix} \tag{3.10}$$
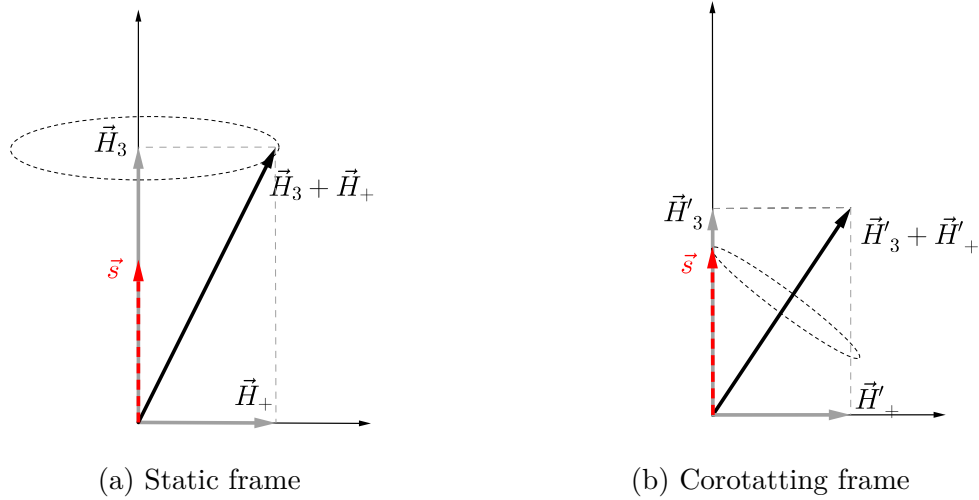

(a) Static frame   (b) Corotatting frame

Figure 3.2: Rabi oscillations in different frames. The vectors $\vec{H}_3$ and $\vec{H}_+$ are defined in Eqn. 3.8. The red dashed vectors are the flavor isospins. The black solid vectors are the vectors that stand for Hamiltonians.

The third component of $\vec{s}$, which is denoted as s_3, is within range $[-1/2, 1/2]$. The two limits, $s_3 = -1/2$ and $s_3 = 1/2$ stand for the two-level system in high energy state and low energy state respectively. If the two-level system has equal

---

[1] The phase ϕ_{R} of the driving potential in Eqn. 3.6 has no effect on the transition probability since it only determines the initial phase of driving Hamiltonian vector $\vec{H}_+$. The oscillation amplitude is not affected by ϕ_{R} at all.

probabilities to be on high energy state and low energy state, I have $s_3 = 0$. The equation of motion is given by Eqn. 2.24. In this example, the total "Hamiltonian vector" $\vec{H}$ is not static since it has a rotating component $\vec{H}_+$. I need a better frame to understand the evolution of the state vector $\vec{s}$.

A more convenient frame is the frame that corotates with $\vec{H}_+$, which is described in Fig. 3.2b. The Hamiltonian in this frame is

$$\frac{\mathrm{d}}{\mathrm{d}t}\vec{s} = \vec{s} \times (\vec{H}'_3 + \vec{H}_+), \tag{3.11}$$

where

$$\vec{H}'_3 = \begin{pmatrix} 0 \\ 0 \\ \omega_\mathrm{R} - k_\mathrm{R} \end{pmatrix}, \qquad \vec{H}'_+ = \begin{pmatrix} A_\mathrm{R} \\ 0 \\ 0 \end{pmatrix}. \tag{3.12}$$

The state vector $\vec{s}$ precesses around the static vector $\vec{H}'_3 + \vec{H}'_+$ in this corotatting frame with a frequency $\Omega_\mathrm{R} = \sqrt{|A_\mathrm{R}|^2 + (k_\mathrm{R} - \omega_\mathrm{R})^2}$. An analysis by projecting the state vector $\vec{s}$ on to the vertical axis shows that

$$s_3 = \frac{1}{2} - \frac{|A_\mathrm{R}|^2}{\Omega_\mathrm{R}^2} \sin^2\left(\frac{\Omega_\mathrm{R}}{2}t\right). \tag{3.13}$$

Such a system has an analytical transition probability from low energy state to high energy state

$$P(t) = \frac{1}{2}(1 - 2s_3(t)) = \frac{|A_\mathrm{R}|^2}{\Omega_\mathrm{R}^2} \sin^2\left(\frac{\Omega_\mathrm{R}}{2}t\right), \tag{3.14}$$

where

$$\Omega_\mathrm{R} = \sqrt{|A_\mathrm{R}|^2 + (k_\mathrm{R} - \omega_\mathrm{R})^2} \tag{3.15}$$

is known as the Rabi frequency. The amplitude A_R is the dominate factor of oscillation frequency when the rabi oscillation is close to resonance. Fig. 3.3 shows two examples of the transition probabilities of Rabi oscillations.

Similar to neutrino oscillations in a uniform matter profile (see Eqn. 2.9), resonance of Rabi oscillations occurs when the term $\vec{H}_3$ disappears in this corotating
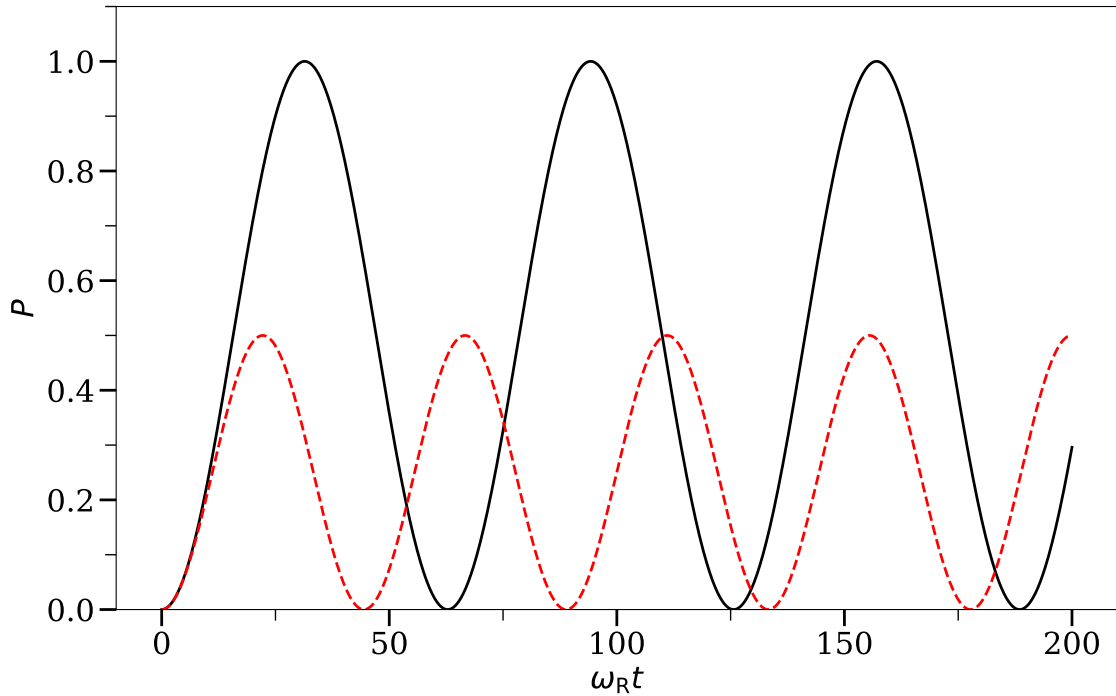
Figure 3.3: Rabi oscillations for two different incoming light frequencies. $k_{\mathrm{R}}/\omega_{\mathrm{R}} = 1$ is the resonance condition. For $k_{\mathrm{R}}/\omega_{\mathrm{R}} = 1.1$, the oscillation amplitude is 0.5. I have used $A_{\mathrm{R}} = 0.1$ in both calculations.

frame. The state vector $\vec{s}$ converts from $+1/2$ (low energy state) to $-1/2$ (high energy state) completely. The detuning, which is defined by $k_{\mathrm{R}} - \omega_{\mathrm{R}}$, determines how off-resonance the system is. The amplitude of driving field A_{R} determines the resonance width,

$$\text{Detuning} = |k_{\mathrm{R}} - \omega_{\mathrm{R}}|, \tag{3.16}$$

$$\text{Resonance Width} = |A_{\mathrm{R}}|. \tag{3.17}$$

The width of the resonance is also explained in Fig. 3.4. We also notice that the transition amplitude is determined by relative detuning D, which is defined as

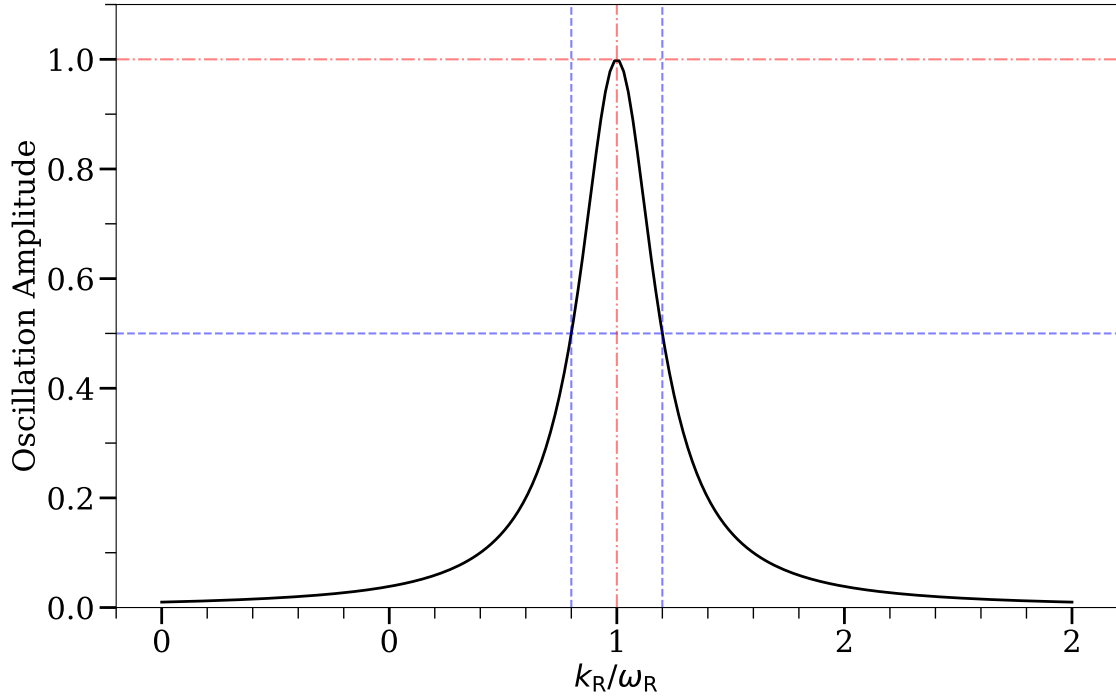$$D = \left| \frac{k_{\mathrm{R}} - \omega_{\mathrm{R}}}{A_{\mathrm{R}}} \right|. \tag{3.18}$$

Figure 3.4: Rabi oscillations for different driving frequencies k_R in unit of ω_R. The maximum amplitude occurs at $k/\omega_0 = 1$. Resonance width is defined to be the width where amplitude becomes half of the maximum which is sandwiched by blue-dashed vertical grid lines. The red-dash-dotted vertical grid line indicates the maximum amplitude.

In many problems, the two-level quantum system has more than one driving frequencies. Here I will explain the Rabi formula that we derived for Rabi oscillation problem with two driving potentials, which has a Hamiltonian of the form

$$
\mathsf{H}_R = -\frac{\omega_R}{2}\sigma_3 - \frac{A_1}{2}\left(\cos(k_1 t + \phi_1)\sigma_1 - \sin(k_1 t + \phi_1)\sigma_2\right)
$$
$$
- \frac{A_2}{2}\left(\cos(k_2 t + \phi_2)\sigma_1 - \sin(k_2 t + \phi_2)\sigma_2\right).
$$

I decompose it into $\vec{H}_R = \vec{H}_3 + \vec{H}_1 + \vec{H}_2$, where

$$
\vec{H}_1 = \begin{pmatrix} A_1 \cos(k_1 t + \phi_1) \\ -A_1 \sin(k_1 t + \phi_1) \\ 0 \end{pmatrix}, \vec{H}_2 = \begin{pmatrix} A_2 \cos(k_2 t + \phi_2) \\ -A_2 \sin(k_2 t + \phi_2) \\ 0 \end{pmatrix}.
$$

Assume $\vec{H}_1$ is the on-resonance perturbation which means that $k_1 = \omega_R$. The three terms are defined as $\vec{H}_3$, $\vec{H}_1$, and $\vec{H}_2$ respectively. $\vec{H}_1$ and $\vec{H}_2$ are two rotating vectors as a function of r with frequencies k_1 and k_2 in this vector space, while $\vec{H}_3$ is perpendicular to $\vec{H}_1$ and $\vec{H}_2$.

The most general condition that we can drop the new perturbation $\vec{H}_2$ is to make sure k_2 is far from the resonance condition compared to the resonance width,

$$D \equiv \frac{|k_2 - \omega_R|}{|A_2|} \gg 1. \tag{3.19}$$

In fact, I will derive a more stringent criteria to neglect the second driving potential using the idea of energy gap shift. To work out the energy gap shift, we go to the frame that corotates with $\vec{H}_2$, in which we have the new frequencies $k_1' = k_1 - k_2$ and $k_2' = 0$ as well as new energy gap $\omega_R' = \omega_R - k_2$. The resonance mode $\vec{H}_1$ retains on the resonance condition since $k_1' = \omega_R'$, i.e. $k_1 - k_2 = \omega_R - k_2$, holds in the new frame. On the other hand, we have two static fields $\vec{H}_3$ and $\vec{H}_2$ together as the new energy gap, as long as $\vec{H}_2 \ll \vec{H}_3$, which is the usual case. The new energy gap in this frame is calculated as

$$\begin{aligned}
\tilde{\omega}_R' &= \text{sign}(\omega_R')\sqrt{\omega_R'^2 + A_2^2} \\
&\approx \omega_R' + \frac{A_2^2}{2\omega_R'} \\
&= \omega_R - k_2 + \frac{1}{2}\frac{A_2^2}{\omega_R - k_2},
\end{aligned} \tag{3.20}$$

where we kept only first order of Taylor series. The Taylor expansion in Eqn. 3.20 holds as long as the relative detuning for the second frequency is large which means the second frequency is off resonance. As an approximation, the transitions between the two energy states follows the Rabi oscillations with energy gap $\tilde{\omega}_R'$ and driving field with frequency $k_1' = k_1 - k_2$. Consequently, we can estimate how much the amplitude of the transition is suppressed due to k_1 mode by calculating the new

relative detuning,

$$
\begin{aligned}
D' &= \frac{|k_1' - \tilde{\omega}_{\mathrm{R}}'|}{|A_1|} \\
&= \left| \frac{k_1 - \omega_{\mathrm{R}}}{A_1} + \frac{A_2^2}{2A_1(k_2 - \omega_{\mathrm{R}})} \right| \qquad (3.21) \\
&= \left| \frac{\mathrm{sign}(k_1 - \omega_{\mathrm{R}})}{\mathrm{sign}(k_2 - \omega_{\mathrm{R}})} D_1 + \frac{A_2}{2A_1 D_2} \right|, \qquad (3.22)
\end{aligned}
$$

where D_1 and D_2 are the relative detuning of the first mode and second mode, respectively. They are defined as

$$
D_i = \left| \frac{k_i - \omega_{\mathrm{R}}}{A_i} \right|.
$$

In principle, the energy gap of the first frequency can be changed to approach the resonance or escape the resonance by carefully arranging the second frequency, which is also obvious from Eqn. (3.22). For the purpose of the section we first discuss the most important destruction effect by choosing $D_1 = 0$. We observe the importance of the relative detuning. For the second mode to significantly interfere with the first mode, we need a small D_2 and a large amplitude or width $A_2 \gg A_1$.

3.3 Single Frequency Matter Profile

I will examine the neutrino flavor conversions in a single frequency matter profile $\delta\lambda(r) = \lambda_1 \cos(k_1 r)$. As will be proved in Sec. 3.5.2, the varying σ_3 term $\delta\lambda(r) \cos 2\theta_{\mathrm{m}} \sigma_3 / 2$ in Hamiltonian Eqn. 3.5, which is the varying energy gap due to varying matter density fluctuations, has little effect on the transition probabilities when the system is not far from resonance. With the varying σ_3 term removed, it indicates that this single frequency matter perturbation neutrino flavor conversion system has been reduced to a Rabi oscillation system, with external driving field frequencies $\pm k_1$ and energy gap ω_{m}. Mathematically, we can decompose $\cos(k_1 r)$ into two exponential functions so that we have two external driving frequencies k_1

and $-k_1$. By neglecting the off-resonance mode which has frequency $-k_1$, the Hamiltonian can be simplified,

$$\mathsf{H}^{(\mathrm{m})} \rightarrow -\frac{\omega_{\mathrm{m}}}{2}\sigma_3 - \frac{1}{2}\lambda_1 \sin 2\theta_{\mathrm{m}} \cos(k_1 r)\sigma_1 \tag{3.23}$$
$$\rightarrow -\frac{\omega_{\mathrm{m}}}{2}\sigma_3 - \frac{1}{2}A_1 \exp(ik_1 r)\sigma_1$$
$$= -\frac{\omega_{\mathrm{m}}}{2}\sigma_3 - \frac{1}{2}A_1 \cos(k_1 r)\sigma_1 + \frac{1}{2}A_1 \sin(k_1 r)\sigma_2,$$

where

$$A_1 = \frac{\lambda_1 \sin 2\theta_{\mathrm{m}}}{2}. \tag{3.24}$$

The resonance condition is determined by matching the energy gap ω_{m} with external driving field frequency k_1, i.e., $\omega_{\mathrm{m}} \sim k_1$. As the system approaches resonance condition, the transition probability between the two mass states should be predicted well using Rabi formula.

To show that this conjecture of simplifying neutrino flavor conversions to Rabi oscillations is correct, we calculate transition probabilities of the neutrinos described by Eqn. 3.5 numerically, and compare them with Rabi formula Eqn. 3.14 from the Rabi oscillations described by Eqn. 3.6.

In Fig. 3.5, I have plotted the numerical results using markers as well as the prediction using Rabi formula using lines. The agreement between numerical solutions of neutrino transitions between mass states and Rabi formula will be explained more precisely in Sec. 3.5. For now, we address the significance of relative detuning $D = |k_1 - \omega_{\mathrm{m}}|/|A_1|$, which is rigoriously defined in Appendix 3.2.1. It measures how off-resonance a system is. $D \rightarrow 0$ indicates that the neutrino oscillation is very close to resonance, while $D \rightarrow \infty$ indicates that the neutrino oscillation is far away from resonance. The corresponding relative detunings are 0, 1.0, and 5.2 for $k_1 = \omega_{\mathrm{m}}$, $k_1 = (1 - 2 \times 10^{-5})\omega_{\mathrm{m}}$, and $k_1 = (1 - 10^{-4})\omega_{\mathrm{m}}$.

For a single-frequency perturbation in the matter profile $\lambda(r) = \lambda_1 + \lambda_1 \sin(k_1 r)$,
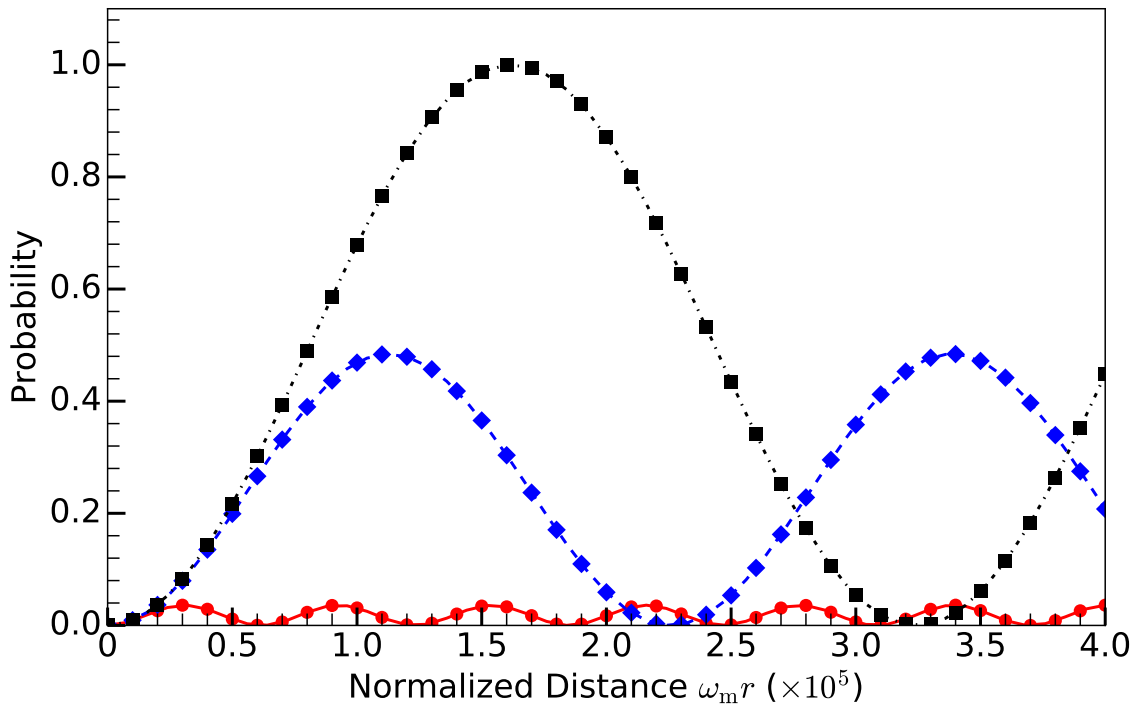
Figure 3.5: Single frequency matter profile and Rabi oscillation. The markers are numerical results for the transition probabilities between two background mass eigenstates for the neutrinos with matter perturbation $A_1 \sin(k_1 r)$. The dots, diamonds, and squares are for $k_1 = \omega_{\mathrm{m}}$, $k_1 = (1 - 2 \times 10^{-5})\omega_{\mathrm{m}}$, and $k_1 = (1 - 10^{-4})\omega_{\mathrm{m}}$ respectively. The lines are the predictions using Rabi formula. During the calculation, λ_0 is set to 0.5 of the MSW resonance potential $\lambda_{\mathrm{MSW}} = \omega_{\mathrm{v}} \cos 2\theta_{\mathrm{v}}$ and mixing angle is chosen so that $\sin^2(2\theta_{\mathrm{v}}) = 0.093$.

P. Krastev and A. Smirnov concluded that the parametric resonance condition is $\omega_{\mathrm{m}} \sim n k_1$, if instantaneous $\omega_{\mathrm{m,inst}}(r)$ associated with the matter profile at distance r varies slowly [5]. This condition is exactly the Rabi resonance condition when $n = 1$, as such condition matches the driving field frequency to the energy split. Higher order effects are explained in Sec. 3.5.2.

3.4   Interference Effects in Multi-frequency Matter Profiles

The approach applied to single frequency matter profile also helps with the understanding of multi-frequency matter profile. However, multi-frequency matter profile leads to multiple modes of Rabi oscillations, even with our simplified approach by dropping the varying σ_3 term in Hamiltonian. In this section, we examine the interference between two modes of Rabi oscillations.

The condition can be verified by comparing the numerical solution and estimation using Rabi formula. However, we are most interested in the amplitude change due to $\mathbf{H}_2$ mode. Relative detuning is the only variable that we need to calculate the amplitude, hence we only compare the numerical results with estimated amplitudes using $1/(1 + D'^2)$. To verify the condition, we choose the first rotating perturbation to satisfy the resonance condition $k_1 = \omega_\mathrm{m}$, the condition for the second rotating field shifting the system out of resonance is that the relative detuning becomes larger than 1, which leads to

$$|A_2| \geq \sqrt{2\omega_\mathrm{m}|A_1(k_2 - \omega_\mathrm{m})|} \equiv A_{2,\mathrm{Critical}}. \tag{3.25}$$

We expect the transition amplitude to decrease as we have larger $|A_2|$.

We choose the two modes where the first one has amplitude $A_1 = 10^{-4}\omega_\mathrm{m}$ and frequency $k_1 = \omega_\mathrm{m}$. With a small amplitude of the second frequency, $A_2 = 10^{-4}\omega_\mathrm{m}$, and large frequency $k_2 = 10\omega_\mathrm{m}$, we obtain almost full resonance. For larger A_2 the destruction effect is more effective, as shown in Fig. 3.6. The estimations of transition amplitude are in good agreement with the numerical results. To show the importance of relative detuning, we calculated the relative detuning for each cases, which are 0.06, 0.6, 1.4, 13.9 for the lines from top to down. We also notice that the width of each cases doesn't change since we kept A_1 fixed for each calculation, which
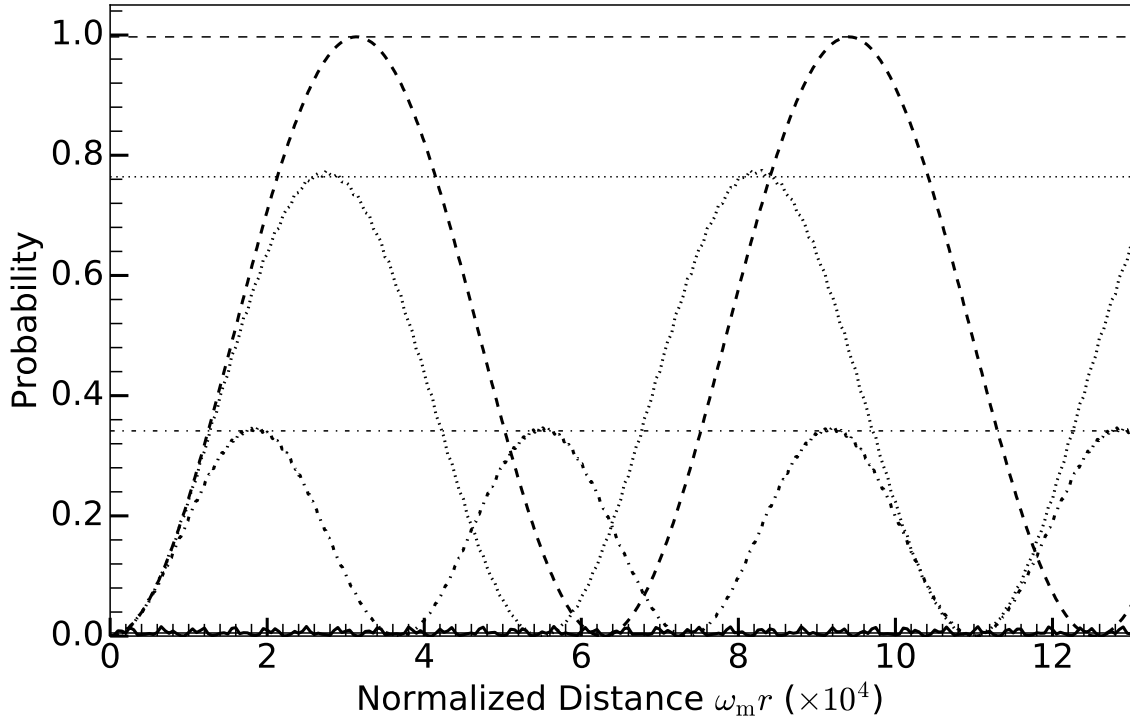
Figure 3.6: Reduction of transition amplitudes due to interference. Dashed line, dotted line, dash-dotted line, and solid line are for $A_2 = 10^{-2}\omega_{\mathrm{m}}$, $k_2 = 10\omega_{\mathrm{m}}$, $A_2 = 10^{-2}\omega_{\mathrm{m}}$, $k_2 = 10^{-1}\omega_{\mathrm{m}}$, $A_2 = 5.0 \times 10^{-2}\omega_{\mathrm{m}}$, $k_2 = 10\omega_{\mathrm{m}}$, and $A_2 = 5 \times 10^{-2}\omega_{\mathrm{m}}$, $k_2 = 10^{-1}\omega_{\mathrm{m}}$. In all the calculations, we choose $A_1 = 10^{-4}\omega_{\mathrm{m}}$, $k_1 = \omega_{\mathrm{m}}$. The grid lines are the transition amplitudes estimated using D'. During the calculation, Λ_0 is set to half of the MSW resonance potential, $\Lambda_0 = \frac{1}{2}\lambda_{\mathrm{MSW}} = \frac{1}{2}\omega_{\mathrm{v}}\cos 2\theta_{\mathrm{v}}$.

indicates that the decreasing in transition amplitude is because of the increasing in detuning.

Even for the single frequency matter profile, there are two modes of Rabi oscillations $\pm k_1$, under the approximation that the varying σ_3 term in Hamiltonian is neglected, as mentioned in Sec. 3.2. The three examples calculated in Fig. 3.5 are almost exact since the modification of relative detuning for the k_1 mode that we kept, due to the far off resonance mode $-k_1$ that we neglected, is tiny. The first two lines of Table. 3.1 show the relative detunings of the three cases in Fig. 3.5, where

$n = \pm 1$ are for the $\pm k_1$ modes in the Hamiltonian Eqn. 3.23. We observe in Fig. 3.5 that the relative detuning change due to an extra $-k_1$ mode is not observable.
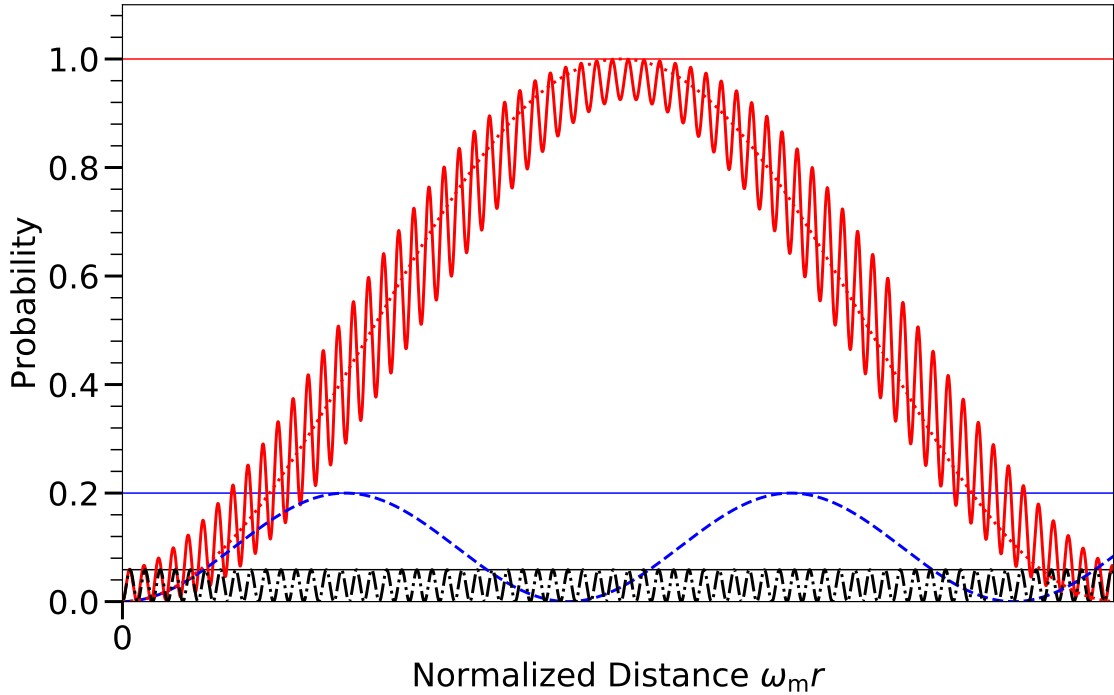

Figure 3.7: Constructive interference for two frequencies in matter density profile. The solid red line, dashed blue line, dash-dotted black line, are the transition probability for two frequencies combined, the first frequency k_1 only, the second frequency k_2 only. The amplitudes of each frequency are $A_1 = 0.4$, $A_2 = 2.6$ respectively. The grid lines are the oscillations amplitudes predicted by Rabi formula. The dotted red line is the oscillations predicted by Rabi formula for the two combined frequencies.

Adding a second frequency to the matter density profile can also be constructive. I calculated an example with two frequencies in matter density profile, so that the Hamiltonian is

$$H^{(m)} = -\frac{\omega_m}{2}\sigma_3 - \left(\frac{A_1}{2}\cos(k_1 r) + \frac{A_2}{2}\cos(k_2 r)\right)\sigma_1 + \left(\frac{A_1}{2}\sin(k_1 r) + \frac{A_2}{2}\sin(k_2 r)\right)\sigma_2.$$

We choose two matter profile frequencies that are off resonance and producing large

relative detuning,

$$A_1 = 0.025, \qquad k_1 = 0.95, \qquad A_1 = 0.4, \qquad k_2 = 2.6. \tag{3.26}$$

The oscillation amplitude for each mode being much smaller than 1. However, the combined two frequencies case produces oscillations are resonance (c.f. Fig. 3.7), since the relative detuning for the combined two frequencies case is 0.

3.5 Parametric Resonance and Rabi oscillation — Jacobi-Anger expansion

With the intuition of the Rabi oscillations itself as well as the interference between different modes of Rabi oscillations shown in Sec. 3.4, I can interpret the transition probabilities of any matter profile more precisely if the system can be exactly decomposed into multiple Rabi oscillations. Kneller et. al provided a method to achieve this goal [20], namely the Jacobi-Anger expansion. In this section, I will show that the matter effect can be decomposed into superpositions of Rabi oscillations by applying a Jacobi-Anger expansion to the Hamiltonian. Our approach is to apply a designed unitary transformation first which make the motivation of Jacobi-Anger expansion, before writing down the final result as superpositions of Rabi oscillation using Jacobi-Anger expansion. For a system with general matter perturbation (see Eqn. 3.5), we apply an unitary transformation of the form

$$\mathsf{U} = \begin{pmatrix} e^{-\mathrm{i}\eta(r)} & 0 \\ 0 & e^{\mathrm{i}\eta(r)} \end{pmatrix}, \tag{3.27}$$

which is a transformation used in Ref. [15] to remove the diagonal elements of the Hamiltonian. This transformation is essentially a rotation $\exp\left(-\mathrm{i}\frac{\sigma_3}{2} \cdot 2\eta\right)$, thus it doesn't change σ_3 terms themselves. In this work, this transformation is used to

remove the varying σ_3 terms $\delta\lambda(r)\cos 2\theta_{\mathrm{m}}\sigma_3/2$ in the Hamiltonian, so that the energy gap is fixed in the new basis $(|\nu_{\mathrm{r1}}\rangle, |\nu_{\mathrm{r2}}\rangle)^{\mathrm{T}}$, which is defined as

$$\begin{pmatrix} |\nu_{\mathrm{r1}}\rangle \\ |\nu_{\mathrm{r2}}\rangle \end{pmatrix} = \mathsf{U}^\dagger \begin{pmatrix} |\nu_{\mathrm{L}}\rangle \\ |\nu_{\mathrm{H}}\rangle \end{pmatrix}. \tag{3.28}$$

For convenience, we name this unitary transformation in Eqn. (3.27) Rabi transformation as well as the new basis in Eqn. (3.28) the Rabi basis. The reason it can remove the σ_3 term is that it will transform the system into a rotating frame so that the varying energy gap due to the fluctuating matter density is exactly cancelled by rotation of the frame. Another advantage of this transformation is that the transition probability from light state to heavy state in background matter basis is easily calculated as $P_{\mathrm{L}\to\mathrm{H}}(x) = |e^{i\eta}\psi_{\mathrm{r2}}(x)|^2 = |\psi_{\mathrm{r2}}(x)|^2$.. In Rabi basis, we find the Schrödinger equation

$$\begin{pmatrix} \frac{\mathrm{d}\eta}{\mathrm{d}r} & 0 \\ 0 & -\frac{\mathrm{d}\eta}{\mathrm{d}r} \end{pmatrix} \begin{pmatrix} \psi_{\mathrm{R1}} \\ \psi_{\mathrm{R2}} \end{pmatrix} + \mathrm{i}\frac{\mathrm{d}}{\mathrm{d}r} \begin{pmatrix} \psi_{\mathrm{R1}} \\ \psi_{\mathrm{R2}} \end{pmatrix}$$
$$= \left[-\frac{\omega_{\mathrm{m}}}{2}\sigma_3 + \frac{\delta\lambda}{2}\cos 2\theta_{\mathrm{m}}\sigma_3 - \frac{\delta\lambda}{2}\sin 2\theta_{\mathrm{m}} \begin{pmatrix} 0 & e^{2i\eta} \\ e^{-2i\eta} & 0 \end{pmatrix} \right] \begin{pmatrix} \psi_{\mathrm{R1}} \\ \psi_{\mathrm{R2}} \end{pmatrix},$$

in which the varying diagonal elements in Hamiltonian can be eliminated by choosing $\eta(r)$ properly, i.e.,

$$\eta(r) - \eta(0) = \frac{\cos 2\theta_{\mathrm{m}}}{2} \int_0^r \delta\lambda(\tau)d\tau. \tag{3.29}$$

In Rabi basis, the Schrödinger equation becomes

$$\mathrm{i}\frac{d}{dr}\begin{pmatrix} \psi_{\mathrm{r1}} \\ \psi_{\mathrm{r2}} \end{pmatrix} = \left[-\frac{\omega_{\mathrm{m}}}{2}\sigma_3 - \frac{\delta\lambda}{2}\sin 2\theta_{\mathrm{m}} \begin{pmatrix} 0 & e^{2i\eta} \\ e^{-2i\eta} & 0 \end{pmatrix} \right] \begin{pmatrix} \psi_{\mathrm{r1}} \\ \psi_{\mathrm{r2}} \end{pmatrix}.$$

One can easily show that the transition probability between two eigenstates in Rabi basis is the same as the transition probability between two eigenstates in background matter basis, given the initial condition that the system is in low energy state.

For single frequency matter profile with potential $\delta\lambda(r) = A_1 \sin(k_1 r)$, we have $\eta(r) = -A_1 \cos 2\theta_{\mathrm{m}} \cos(k_1 r)/(2k)$. To make connection with Rabi oscillation, we apply Jacobi-Anger expansion, which is used in Ref. [20], to decompose the $\exp\left(iz \cos\left(k_1 r\right)\right)$-like term in Hamiltonian into linear combinations of terms that is proportional to $\exp\left(ink_1 r\right)$, i.e., to decompose spherical waves into plane waves. The decomposed form of Hamiltonian explicitly shows that the Hamiltonian is a summation of Rabi systems, which is

$$\mathsf{H}^{(\mathrm{R})} = -\frac{\omega_{\mathrm{m}}}{2}\sigma_3 - \frac{1}{2}\sum_{n=-\infty}^{\infty} B_n \begin{pmatrix} 0 & \Phi_n e^{ink_1 r} \\ \Phi_n^* e^{-ink_1 r} & 0 \end{pmatrix}, \tag{3.30}$$

where

$$B_n = \tan 2\theta_{\mathrm{m}} n k_1 J_n\left(\frac{A_1}{k_1}\cos 2\theta_{\mathrm{m}}\right), \tag{3.31}$$

$$\Phi_n = e^{i\pi(3n/2+1)}, \tag{3.32}$$

with J_n standing for the Bessel function. The constant phase Φ_n doesn't play any role for the reason discussed in Appendix 3.2.1. Phase in matter potential would also go into Φ_n, for which reason, phase of matter profile is not included in the current discussion. In the Hamiltonian, the first term describes the energy gap, while the second term is the summation of many driving fields. The resonance width for a given mode n is $|B_n|$. It's worth mentioning that we have [17]

$$J_n(n\,\mathrm{sech}\,\alpha) \sim \frac{e^{n(\tanh\alpha-\alpha)}}{\sqrt{2\pi n \tanh\alpha}} \tag{3.33}$$

for large n. It's straightforward to prove that resonance width decreases dramatically for large n thus resonance of higher order modes become insignificant.

When the system has one dominate resonance mode and without significant interference between the resonance mode and other modes, all off-resonance modes can be dropped without significantly changing the transition probabilities. However, as we have shown previously in Sec. 3.4, interference might happen between different

modes and interferences were measured with a criteria. However, interference is not the only effect we need to consider. The following subsections will determine the important modes of the system (i.e., which n to include) and explore the interference between modes hence explain the coincidence presented in the previous sections. We use dimensionless quantities which are scaled using the characteristic energy scale ω_{m}, e.g.,

$$\hat{r} = \omega_{\mathrm{m}} r, \qquad \hat{k}_1 = \frac{k_1}{\omega_{\mathrm{m}}}, \qquad \hat{A}_1 = \frac{A_1}{\omega_{\mathrm{m}}}, \qquad \hat{B}_n = \frac{B_n}{\omega_{\mathrm{m}}}. \tag{3.34}$$

3.5.1 The Relative Detuning

In order for a mode to have a significant effect on the transition probabilities, we require it to has large relative detuning D, and a large oscillation wavelength compared to the size of the physical system. Relative detuning for each mode is calculated as

$$D_n = \frac{|nk_1 - \omega_{\mathrm{m}}|}{B_n} \tag{3.35}$$

for single frequency matter profile, and

$$D_{\{n_a\}} = \frac{|\sum_a n_a k_a - \omega_{\mathrm{m}}|}{B_{\{n_a\}}} \tag{3.36}$$

for multi-frequency matter profile.

For modes with small relative detuning, they are important since they might lead to full transition. However, the full transition requires at least a distance of the order of the wavelength of the oscillation. Suppose we have a mode that has zero relative detuning, but with a oscillation wavelength much larger than the size of the system, such a mode would never have the chance to accumulate a large transition probability within the size of the system. By utilizing the theory of Rabi oscillation, we know that the oscillation wavelength of each mode is determined by the Rabi frequency

$$\Omega_{\{n_a\}} = |B_{\{n_a\}}| \sqrt{1 + D_{\{n_a\}}^2}. \tag{3.37}$$

Thus modes that has much larger oscillation wavelength are not subjected to be considered even though their relative detunings are close to zero.

In principle, we can always approximate the system by including more modes with larger relative detuning while neglecting the modes with wavelength much longer than the size of physical system. However such effort doesn't simplify the calculations.

3.5.2 Single Frequency Matter Profile Revisited

For the single frequency matter potential $\lambda = \lambda_0 + \lambda_1 \sin(k_1 r)$ discussed in Sec. 3.2, we removed the varying σ_3 term by arguing that this term has no effect on transition probabilities when the system is close to resonance, $k_1 \sim \omega_{\mathrm{m}}$. The reason is that only the first mode $n = 1$ is on resonance when $k_1 = \omega_{\mathrm{m}}$ and all other modes are far from resonance, thus

$$
\mathsf{H}^{\mathrm{R}} \approx -\frac{\omega_{\mathrm{m}}}{2}\sigma_3 - \frac{1}{2}B_1 \begin{pmatrix} 0 & \Phi_1 e^{ik_1 r} \\ \Phi_1^* e^{-ik_1 r} & 0 \end{pmatrix} \tag{3.38}
$$
$$
\approx -\frac{\omega_{\mathrm{m}}}{2}\sigma_3 - \frac{A_1}{2}\cos(k_1 r)\sigma_1 + \frac{A_1}{2}\sin(k_1 r)\sigma_2,
$$

where A_1 is defined in Eqn. (3.24) and approximation

$$
J_1\left(\frac{\lambda_1}{k_1}\cos(2\theta_{\mathrm{m}})\right) \approx \frac{\lambda_1}{2k_1}\cos(2\theta_{\mathrm{m}})
$$

for $\lambda_1 \cos(2\theta_{\mathrm{m}})/k_1 \ll 1$ is used in the last step. Thus we reach a similar equation to the approximation we used in Sec. 3.2. $\lambda_1 \cos(2\theta_{\mathrm{m}})/k_1 \ll 1$ corresponds to small resonance width for Eqn. (3.23) and also Eqn. (3.38) so that the interferences are small.

Using Jacobi-Anger expansion, we can calculate the relative detuning for each mode as well as the interference effect. The relative detuning for each mode in the Jacobi-Anger expansion for single frequency matter profile used in Fig. 3.5 is

	$k_1 = \omega_m$				$k_1 = (1 - 2 \times 10^{-5})\omega_m$				$k_1 = (1 - 10^{-4})\omega_m$		
n	D	D_1'	$2\pi\omega_m/\Omega_n$	n	D	D_1'	$2\pi\omega_m/\Omega_n$	n	D	D_1'	$2\pi\omega_m/\Omega_n$
1	0	-	3.2×10^5	1	1	-	2.2×10^5	1	5.2	-	6.2×10^4
-1	10^5	4.8×10^{-6}	3.1	-1	10^5	1	3.1	-1	10^5	5.2	3.1
2	1.1×10^9	2.1×10^{-14}	6.3	2	1.1×10^9	1	6.3	2	1.1×10^9	5.2	6.3
-2	3.4×10^9	6.9×10^{-15}	2.1	-2	3.4×10^9	1	2.1	-2	3.4×10^9	5.2	2.1

Table 3.1: Relative detuning and oscillation wavelength of each mode for single frequency matter profile.

calculated and listed in Table. 3.1. The D_1' is the shifted relative detuning of the first mode with $n = 1$ due to other mode. It clearly shows that the first mode takes the whole system so that the approximation of neglecting the varying σ_3 terms in Hamiltonian is accurate enough. One can also show that the interference effect due to higher order modes is negligible, since they do not change the relative detuning of the most significant modes.

The rigorous solutions for each modes in Eqn. 3.30 is obtained,

$$P_{L \to H}^{(n)} = \frac{\left|\hat{B}_n\right|^2}{\left|\hat{B}_n\right|^2 + (n\hat{k} - 1)^2} \sin^2\left(\frac{\hat{q}^{(n)}}{2}\hat{x}\right), \tag{3.39}$$

where

$$\Gamma^{(n)} = \left|\hat{B}_n\right|, \quad \text{width of resonance } (n\hat{k} \text{ as parameter}) \tag{3.40}$$

$$\hat{q}^{(n)} = \sqrt{\left|\Gamma^{(n)}\right|^2 + (n\hat{k} - 1)^2}, \quad \text{frequency of oscillations.} \tag{3.41}$$

The impact of detuning is also verified in Fig. 3.8. The example clearly shows the width of the resonance is dropping dramatically for larger modes in Jacobi-Anger expansion. A careful investigation shows that the resonance width is dropping exponentially as shown in Fig. 3.9 and Fig. 3.10.
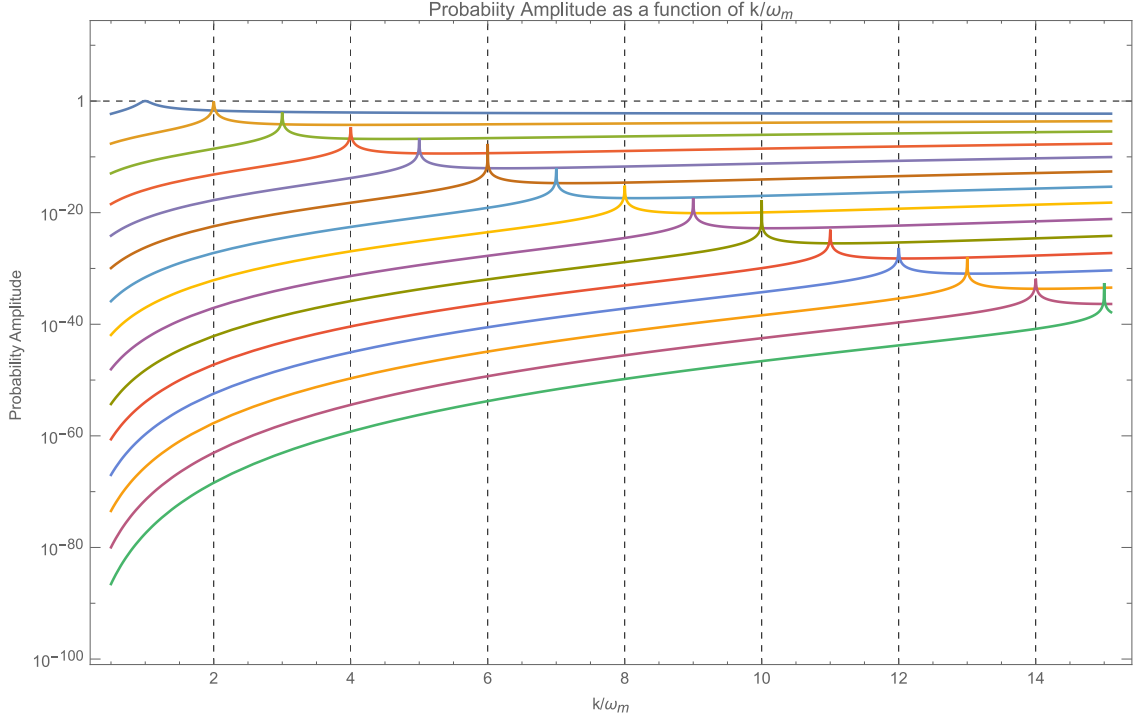
Figure 3.8: Probability amplitude as a function of k/ω_{m} for each term in Jacobi-Anger expansion, with parameters $\lambda_1 = 0.1, \theta_{\mathrm{m}} = \pi/5$.

3.5.3   Castle Wall Matter Profile

For completeness of this chapter, we show one example of multi-frequency matter profile. One of the multi-frequency matter profiles that has been well studied is the castle wall matter profile. Using Fourier series, any matter profile can be Fourier decomposed into superposition of many single frequency matter profile in principle. We decompose the periodic castle wall matter profile into many frequencies and study the interference effect. The potential shown in Fig. 3.11 is defined as,

$$\lambda(r) = \begin{cases} \Lambda_1, & -\frac{X_1}{2} + nX \leq r \leq \frac{X_1}{2} + nX \\ \Lambda_2, & \frac{X_1}{2} + nX \leq r \leq \frac{X_1}{2} + \frac{X_2}{2} + nX \end{cases} \quad (3.42)$$
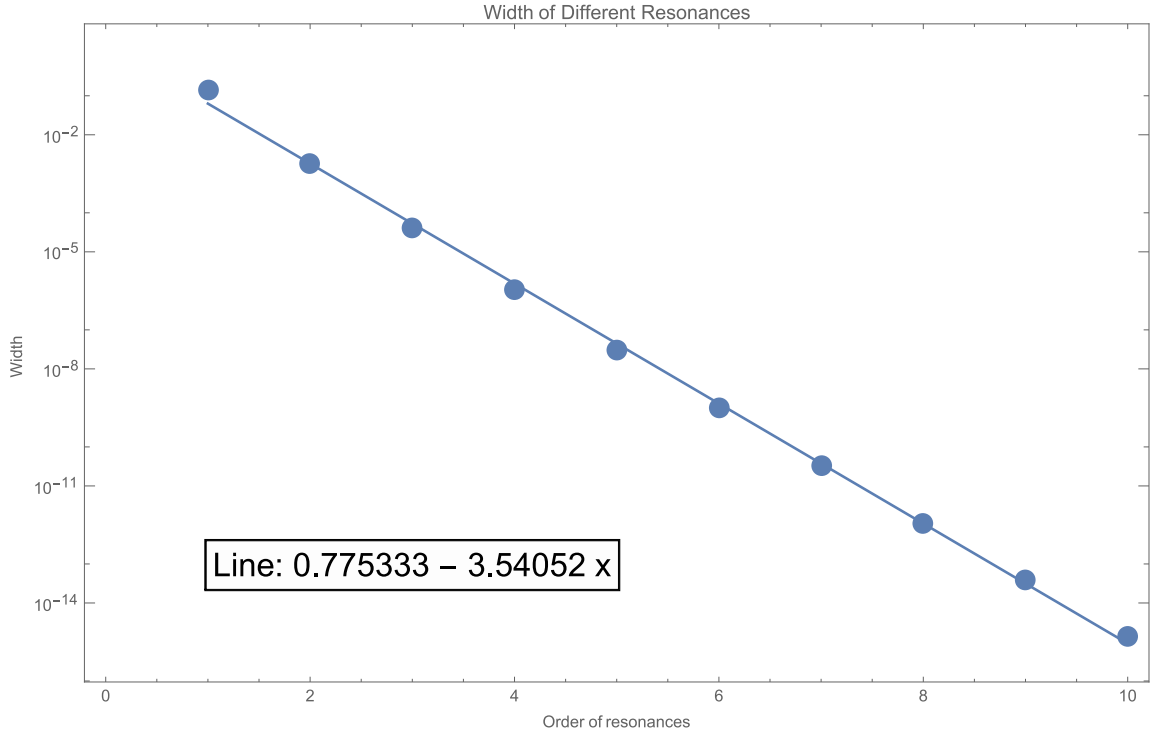
43

Figure 3.9: Resonance width as a function of mode order for each term in Jacobi-Anger expansion, with parameters $\lambda_1 = 0.1, \theta_m = \pi/5$.

where X_1 and X_2 are the two periods of the matter profile or potential, $X = X_1 + X_2$, and n is integer. The parametric resonance condition derived by E. Akhmedov [8] is,

$$\frac{\tan(\omega_{m1}X_1/2)}{\tan(\omega_{m2}X_2/2)} = -\frac{\cos 2\theta_{m2}}{\cos 2\theta_{m1}}, \tag{3.43}$$

where ω_{mi} and θ_{mi} are the energy difference and mixing angle for potential Λ_1 and Λ_2 respectively.

Even though this castle wall problem is analytically solved, the resonance condition Eqn. (3.43) itself is not transparent. In this subsection, we show that such a system is closed related to Rabi oscillations. For illustration purpose, we set the profile to be equal period for the two densities so that $X_1 = X_2 \equiv X/2$. To show that the neutrino flavor conversions in this castle wall matter profiles is related to
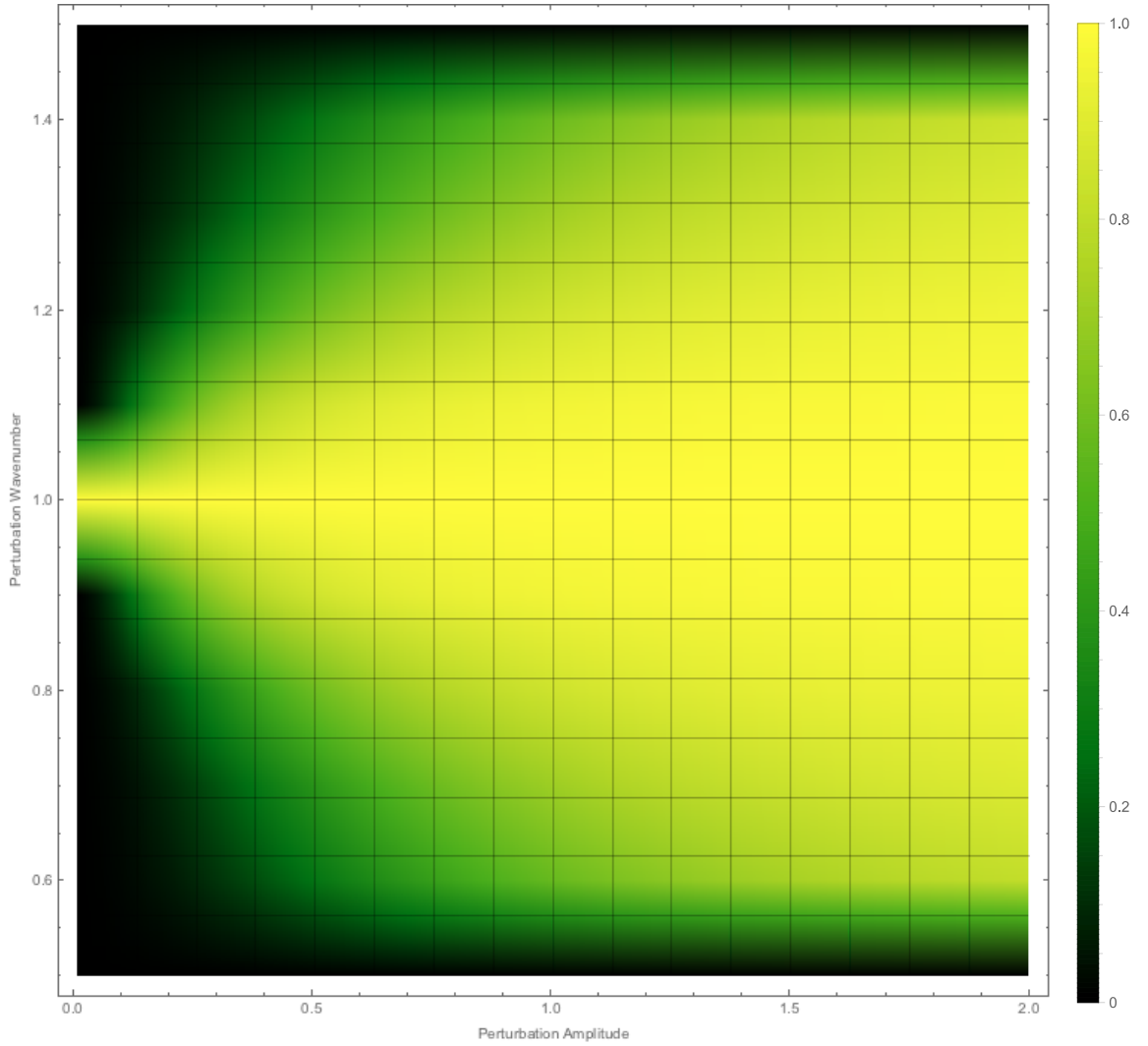
Figure 3.10: Transition probability amplitude at different perturbation amplitude and perturbation wavenumber. Larger amplitudes corresponds to larger resonance width, as another confirmation to Fig. 3.9.

Rabi oscillation, we decompose the profile using Fourier series,

$$\lambda(r) = \lambda_0 + \sum_{n=1}^{\infty} \lambda_n \cos(k_n r), \tag{3.44}$$

where

$$\lambda_0 = (\Lambda_1 + \Lambda_2)/2,$$

$$\lambda_n = \frac{2}{(2n-1)\pi}(-1)^n (\Lambda_1 - \Lambda_2),$$

$$k_n = (2n-1)k_0,$$

$$k_0 = 2\pi/X.$$

The decomposition is visualized in Fig. **??**.

To calculate the transitions between two mass states of background matter potential λ_0, we use the background matter basis with respect to λ_0, in which the transition is zero when varying matter profile vanishes. The Hamiltonian

$$\mathsf{H}^{(\mathrm{m})} = -\frac{1}{2}\omega_{\mathrm{m}}\sigma_3 + \frac{1}{2}\sum_{n=1}^{\infty}\lambda_n \cos 2\theta_{\mathrm{m}} \cos(k_n r)\,\sigma_3 - \frac{1}{2}\sum_{n=1}^{\infty}\lambda_n \sin 2\theta_{\mathrm{m}} \cos(k_n r)\,\sigma_1, \quad (3.45)$$

determines the transitions between the two background matter states.

The base frequency k_0 which is determined by the total period X can be arbitrary. In this example, we choose a X so that the base frequency k_0 matches the energy gap ω_{m}. Even though multiple perturbation frequencies show up in Eqn. (3.45), we identify that only the first frequency $n = 1$ is the resonance frequency since we are using $k_0 = \omega_{\mathrm{m}}$. As an approximation, we drop all other frequencies $n > 2$ regarding the fact that they are far from resonance. Thus, similar to single frequency matter profile, the varying σ_3 terms have limited effects on the transition probabilities in our case, which leads to

$$H^{(\mathrm{m})} \to -\frac{1}{2}\omega_{\mathrm{m}}\sigma_3 - \frac{1}{2}\sum_{n=1}^{2}\lambda_n \sin 2\theta_{\mathrm{m}} \cos(k_n r)\,\sigma_1$$

$$\to -\frac{1}{2}\omega_{\mathrm{m}}\sigma_3 - \frac{1}{2}\sum_{n=1}^{2}A_n \cos(k_n r)\sigma_1$$

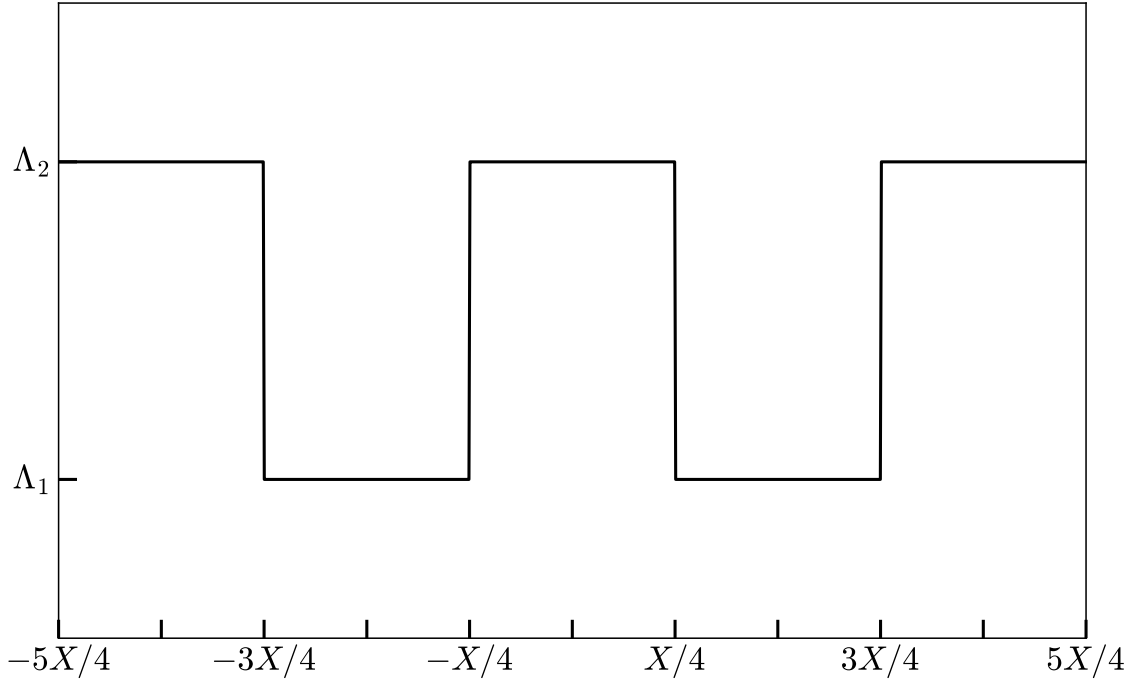$$+ \frac{1}{2}\sum_{n=1}^{2}A_n \sin(k_n r)\sigma_2,$$

Figure 3.11: The castle wall matter potential profile with $X_1 = X_2 = X/2$.

where

$$A_n = \frac{\lambda_n \sin 2\theta_{\mathrm{m}}}{2}.$$

The relative detuning is 0 if we have only the first mode. However, it becomes

$$D'_1 = \frac{A_2^2}{2|A_1(\omega_{\mathrm{m}} - k_2)|}, \tag{3.46}$$

if we include the second frequency k_2. One feature of this Fourier series expanded matter profile Eqn. (3.44) is that the width of each frequency decreases as the order n increases while the detuning of each frequency increases. We calculate the relative detuning for each frequency

$$D_n = \frac{|k_n - \omega_{\mathrm{m}}|}{|\lambda_n \sin 2\theta_{\mathrm{m}}/2|} = \frac{2(n-1)(2n-1)\pi\omega_{\mathrm{m}}}{(\Lambda_2 - \Lambda_1) \sin 2\theta_{\mathrm{m}}} \tag{3.47}$$

which is quadratic in n and inversely proportional to $\Lambda_2 - \Lambda_1$. We find that all higher frequencies k_n for $n > 2$ have very large relative detunings. The neutrino transition
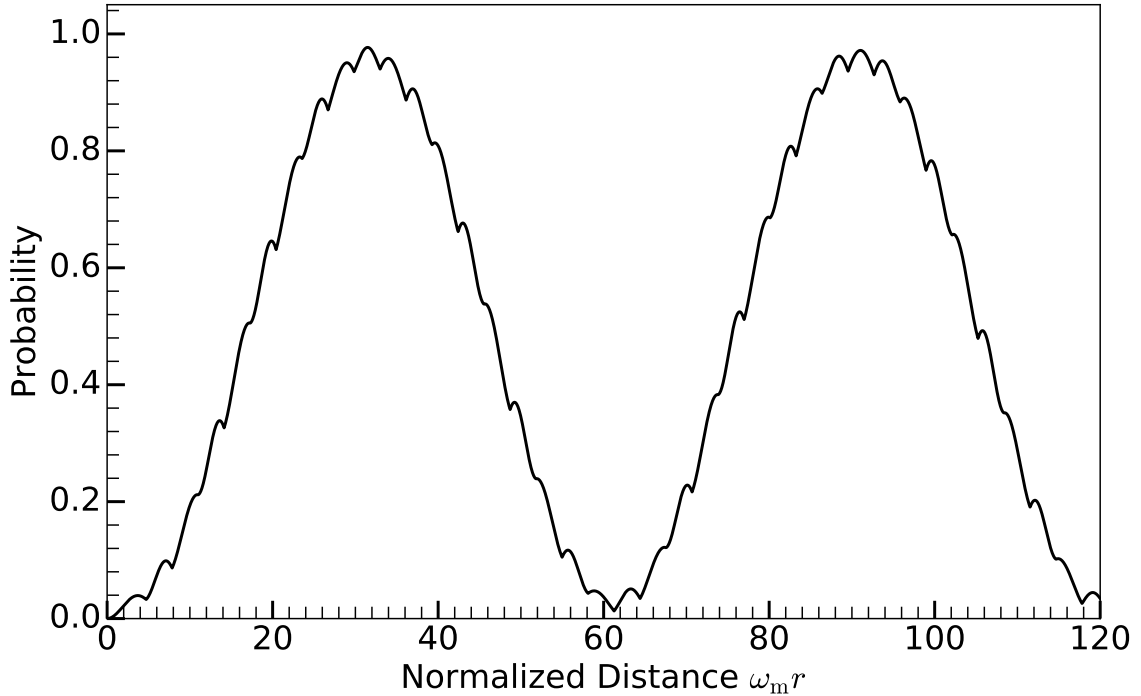
Figure 3.12: Transition probabilities for castle wall matter profile calculated numerically for $\Lambda_2 - \Lambda_1 = 0.4\Lambda_0$. During the calculation, the energy of neutrinos is $10\,\text{MeV}$, mass-squared difference is $\delta m^2 = 2.6 \times 10^{-3}\,\text{eV}^2$, and the vacuum mixing angle chosen so that $\sin^2(2\theta_\text{v}) = 0.093$. The background potential Λ_0 is chosen so that it's half the MSW resonance potential, $\Lambda_0 = \frac{1}{2}\lambda_\text{MSW} = \frac{1}{2}\omega_\text{v}\cos 2\theta_\text{v}$, and the base frequency is set to $k_0 = 2\pi/X = \omega_\text{m}$.

probability between the two matter states is shown in Fig. 3.12, where we find the system has almost full transition.

A more rigorous treatment is to use Jacobi-Anger expansion and find the Rabi modes, where we find that the mode that corresponds to single frequency k_1 dominates and all other modes have little destruction effect on it. Quantitatively, higher orders leads to smaller width $B_{\{n_i\}}$ yet larger detuning $\sum_n nk_n - \omega_\text{m}$, which renders a smaller effect on the resonance mode $\{1, 0\}$, since the effect is evaluated as Eqn. (3.22). Table 3.2 lists the first few smallest relative detunings of Fig. 3.12. The second column is the relative detuning of the corresponding mode, while the third

$\{n_1, n_2\}$	D	$D'_{\{1,0\}}$
$\{1, 0\}$	0	-
$\{-1, 0\}$	48	1.0×10^{-2}
$\{0, 1\}$	1.5×10^2	1.1×10^{-3}
$\{2, 0\}$	2.4×10^2	2.0×10^{-4}

Table 3.2: Relative detuning of each frequency.

column is the relative detuning of mode $\{1, 0\}$ with the energy gap shift effect of the corresponding mode.

3.6 Deep Diving into Jacobi-Anger Expansion

3.6.1 Single Matter Density Frequencies

As a first step, we solve single frequency matter perturbation

$$\delta\lambda(x) = A\sin(kx + \phi). \tag{3.48}$$

Using the relation between η and $\delta\lambda$, we solve out η.

$$\eta(x) = -\frac{\omega_{\mathrm{m}}}{2}x - \frac{\cos 2\theta_{\mathrm{m}}}{2}\frac{A}{k}\cos(kx + \phi), \tag{3.49}$$

where we have chosen $\eta(0) = -\frac{\cos 2\theta_{\mathrm{m}}}{2}\frac{A}{k}\cos\phi$. The problem is to solve the equation of motion

$$i\frac{d}{dx}\begin{pmatrix}\psi_{b1}\\\psi_{b2}\end{pmatrix} = \frac{\sin 2\theta_{\mathrm{m}}}{2}\delta\lambda(x)\begin{pmatrix}0 & e^{2i\eta(x)}\\e^{-2i\eta(x)} & 0\end{pmatrix}\begin{pmatrix}\psi_{b1}\\\psi_{b2}\end{pmatrix}. \tag{3.50}$$

We also define

$$h = \frac{\sin 2\theta_{\mathrm{m}}}{2}\delta\lambda(x)e^{2i\eta(x)} \tag{3.51}$$

$$= \frac{\sin 2\theta_{\mathrm{m}}}{2}A\sin(kx + \phi)e^{i\left(-\omega_{\mathrm{m}}x - \frac{A\cos 2\theta_{\mathrm{m}}}{k}\cos(kx+\phi)\right)}, \tag{3.52}$$

so that the equation of motion becomes

$$i\frac{d}{dx}\begin{pmatrix} \psi_{b1} \\ \psi_{b2} \end{pmatrix} = \begin{pmatrix} 0 & h \\ h^* & 0 \end{pmatrix}\begin{pmatrix} \psi_{b1} \\ \psi_{b2} \end{pmatrix}. \tag{3.53}$$

We apply Jacobi-Anger expansion, c.f. Eqn. **??**, to rewrite the exponential into some plane wave terms [21].

We define $z_k = \frac{A}{k}\cos 2\theta_{\mathrm{m}}$, with which we expand the term

$$e^{-i\frac{\cos 2\theta_{\mathrm{m}} A}{k}\cos(kx+\phi)} = \sum_{n=-\infty}^{\infty} i^n J_n(-z_k)e^{in(kx+\phi)} = \sum_{n=-\infty}^{\infty} (-i)^n J_n(z_k)e^{in(kx+\phi)}, \tag{3.54}$$

where I used $J_n(-z_k) = (-1)^n J_n(z_k)$ for integer n. The expansion is plugged into the Hamiltonian elements,

$$h = \frac{A\sin 2\theta_{\mathrm{m}}\sin(kx+\phi)}{2}e^{-i\omega_{\mathrm{m}}x}\sum_{n=-\infty}^{\infty}(-i)^n J_n(z_k)e^{in(kx+\phi)} \tag{3.55}$$

$$= \frac{A\sin 2\theta_{\mathrm{m}}}{4i}\left(e^{i(kx+\phi)} - e^{-i(kx+\phi)}\right)e^{-i\omega_{\mathrm{m}}x}\sum_{n=-\infty}^{\infty}(-i)^n J_n(z_k)e^{in(kx+\phi)} \tag{3.56}$$

$$= \frac{A\sin 2\theta_{\mathrm{m}}}{4i}\left(\sum_{n=-\infty}^{\infty} e^{i(n+1)}i^n J_n(z_k)e^{i((n+1)k-\omega_{\mathrm{m}})x} - \sum_{n'=-\infty}^{\infty} e^{i(n'-1)}(-i)^{n'} J_{n'}(z_k)e^{i((n'-1)k-\omega_{\mathrm{m}})x}\right)$$
$$\tag{3.57}$$

$$= \frac{A\sin 2\theta_{\mathrm{m}}}{4}\sum_{n=-\infty}^{\infty} e^{in\phi}\left(-(-i)^n\right)\frac{2n}{z_k}J_n(z_k)e^{i(nk-\omega_{\mathrm{m}})x}, \tag{3.58}$$

where I have used

$$J_{n-1}(z_k) + J_{n+1}(z_k) = \frac{2n}{z_k}J_n(z_k). \tag{3.59}$$

Here comes the approximation. The most important oscillation we need is the one with largest period, which indicates the phase to be almost zero,

$$(n+1)k - \omega_{\mathrm{m}} \sim 0 \tag{3.60}$$

$$(n'-1)k - \omega_{\mathrm{m}} \sim 0. \tag{3.61}$$

The two such conditions for the two summations are

$$n \equiv n_- = \text{Int}\left(\frac{\omega_m}{k}\right) - 1 \tag{3.62}$$

$$n' \equiv n_+ = \text{Int}\left(\frac{\omega_m}{k}\right) + 1. \tag{3.63}$$

We define $\text{Int}\left(\frac{\omega_m}{k}\right) = n_0$,

$$n_- = n_0 - 1 \tag{3.64}$$

$$n_+ = n_0 + 1. \tag{3.65}$$

The element of Hamiltonian is written as

$$h = -\frac{A \sin 2\theta_m}{2} e^{in_0\phi}(-i)^{n_0} \frac{n_0}{z_k} J_{n_0}(z_k) e^{i(n_0 k - \omega_m)x}. \tag{3.66}$$

To save keystrokes, we define

$$F = -A \sin 2\theta_m e^{in_0\phi}(-i)^{n_0} \frac{n_0}{z_k} J_{n_0}(z_k), \tag{3.67}$$

which depends on n_0 and $z_k = \frac{A}{k}\cos 2\theta_m$. Notice that

$$|F|^2 = |k \tan 2\theta_m n_0 J_{n_0}(z_k)|^2. \tag{3.68}$$

Thus the 12 element of the Hamiltonian is rewritten as

$$h = \frac{1}{2} F e^{i(n_0 k - \omega_m)x}. \tag{3.69}$$

The general solution to the equation of motion is

$$\psi_{b1} = C_1 e^{\frac{1}{2}i\left(n_0 k - \omega_m - \sqrt{|F|^2 + (n_0 k - \omega_m)^2}\right)x} + C_2 e^{\frac{1}{2}i\left(n_0 k - \omega_m + \sqrt{|F|^2 + (n_0 k - \omega_m)^2}\right)x} \tag{3.70}$$

$$\psi_{b2} = \frac{C_1}{F^*} i\left(n_0 k - \omega_m - \sqrt{|F|^2 + (n_0 k - \omega_m)^2}\right) e^{-\frac{1}{2}i(n_0 k - \omega_m)x - \frac{1}{2}i\sqrt{|F|^2 + (n_0 k - \omega_m)^2}}$$

$$+ \frac{C_2}{F^*} i\left(n_0 k - \omega_m + \sqrt{|F|^2 + (n_0 k - \omega_m)^2}\right) e^{-\frac{1}{2}i(n_0 k - \omega_m)x + \frac{1}{2}i\sqrt{|F|^2 + (n_0 k - \omega_m)^2}}. \tag{3.71}$$

For simplicity, we define

$$g = n_0 k - \omega_{\mathrm{m}}, \tag{3.72}$$

$$q^2 = |F|^2 + g^2. \tag{3.73}$$

To determine the constants, we need initial condition,

$$\begin{pmatrix} \psi_1(0) \\ \psi_2(0) \end{pmatrix} = \begin{pmatrix} 1 \\ 0 \end{pmatrix}, \tag{3.74}$$

which leads to

$$\begin{pmatrix} \psi_{b1}(0) \\ \psi_{b2}(0) \end{pmatrix} = \begin{pmatrix} e^{i\eta(0)} \\ 0 \end{pmatrix}. \tag{3.75}$$

Plug in the initial condition for the wave function,

$$C_1 + C_2 = e^{i\frac{z_k}{2}\cos\phi} \tag{3.76}$$

$$\frac{C_1}{2F^*}i(g-q) + \frac{C_2}{F^*}i(q+g) = 0. \tag{3.77}$$

The constants are solved out

$$C_1 = e^{i\frac{z_k}{2}\cos\phi}\frac{q+g}{2q}, \tag{3.78}$$

$$C_2 = e^{i\frac{z_k}{2}\cos\phi}\frac{q-g}{2q}. \tag{3.79}$$

where F is defined in 3.67 and l and g are defined in 3.73. The second element of wave function becomes

$$\psi_{b2}(x) = \frac{-F}{q}e^{i\frac{z_k}{2}\cos\phi}e^{-\frac{i}{2}gx}\sin\left(\frac{1}{2}qx\right). \tag{3.80}$$

The transition probability becomes

$$P_{1\to2} = |\psi_{b2}|^2 = \frac{|F|^2}{q^2}\sin^2\left(\frac{q}{2}x\right), \tag{3.81}$$

where q is the oscillation wavenumber. Period of this oscillation is given by $T = \frac{2\pi}{q}$.

Compared to the results by Kneller et al [20], where the transition probability is

$$P_{12} = \frac{\kappa_n^2}{q_n^2} \sin^2(q_n x),$$

(3.82)

where $q_n^2 = k_n^2 + \kappa_n^2$ and $2k_n = \tilde{\delta k}_{12} + nk_\star$.

In my notation, k is the same as their $k_\star$. After the first step of translation, we have $g = 2k_n$.

The definition of κ_n is given by

$$\kappa_{ij,n} = (-i)^{n-1} \frac{nC_\star V_\star}{z_{ij}} J_n(z_{ij}) \tilde{U}_{ei}^* \tilde{U}_{ej} e^{i(n\eta + z_{ij} \cos \eta)},$$

(3.83)

in Kneller et al's notation and

$$\delta V_{ee}(x) = C_\star V_\star \sin(k_\star x + \eta).$$

(3.84)

So we conclude that my $|F|^2$ is related to Kneller et al's $|\kappa_n|^2$ through

$$|F|^2 = 4|\kappa_n|^2.$$

(3.85)

We also have

$$q^2 = |F|^2 + g^2 = 4q_n^2,$$

(3.86)

i.e., $q_n = \frac{q}{2}$. Now we see the method we have used gives exactly the same transition probability as Kneller et al's.

To make the numerical calculations easier, we rewrite the result by defining the scaled variables

$$\hat{x} = \omega_{\mathrm{m}} x,$$

(3.87)

$$\hat{k} = \frac{k}{\omega_{\mathrm{m}}},$$

(3.88)

$$\hat{A} = \frac{A}{\omega_{\mathrm{m}}},$$

(3.89)

$$\hat{g} = \frac{g}{\omega_{\mathrm{m}}} = n_0 \hat{k} - 1,$$

(3.90)

$$\hat{q} = \sqrt{|\hat{F}|^2 + \hat{g}^2} = \sqrt{|\hat{k} \tan 2\theta_{\mathrm{m}} n_0 J_{n_0}(z_k)| + \hat{g}^2},$$

(3.91)

Hamiltonian	Solution to The First Element of Wave Function
$-\frac{\omega_{\mathrm{m}}}{2}\sigma_3$	$\psi_1 \sim e^{i\omega_{\mathrm{m}}x/2}$
$\frac{\delta\lambda}{2}\cos 2\theta_{\mathrm{m}}\sigma_3$	$\psi_1 \sim e^{i\frac{A\cos 2\theta_{\mathrm{m}}}{2k}\cos(kx+\phi)}$
$\frac{\delta\lambda}{2}\cos 2\theta_{\mathrm{m}}\sigma_3$	$\psi_1 = C_1 e^{i\frac{A\sin 2\theta_{\mathrm{m}}}{2k}\cos(kx+\phi)} + C_2 e^{-i\frac{A\sin 2\theta_{\mathrm{m}}}{2k}\cos(kx+\phi)}$

Table 3.3: Each terms in Hamiltonian and the corresponding solutions to the specific term.

so that $n_0 = \mathrm{Round}\left(1/\hat{k}\right)$, $z_k = \frac{\hat{A}}{\hat{k}}\cos 2\theta_{\mathrm{m}}$ and

$$P_{1\to 2} = \frac{\left|\hat{k}\tan 2\theta_{\mathrm{m}}n_0 J_{n_0}(z_k)\right|^2}{\left|\hat{k}\tan 2\theta_{\mathrm{m}}n_0 J_{n_0}(z_k)\right|^2 + \hat{g}^2}\sin^2\left(\frac{\hat{q}}{2}\hat{x}\right). \tag{3.92}$$

Mathematical Analysis of The Result

There are several question to answer before we can understand the picture of the math.

- What does each term mean in the Hamiltonian?

- What exactly is the unitary transformation we used to rotate the wave function?

- What is the physical meaning of Jacobi-Anger expansion in our calculation?

To answer the first question, we need to write down the solution to Schrodinger equation assuming the Hamiltonian has only one term. The results are listed below in Table 3.3.

The unitary transformation used is to move our reference frame to a co-rotating one. $-\frac{\omega_{\mathrm{m}}}{2}\sigma_3$ is indeed causing the wave function to rotate and removing this term using a transformation means we are co-rotating with it. $\frac{\delta\lambda}{2}\cos 2\theta_{\mathrm{m}}\sigma_3$ causes a more complicated rotation however it is still a rotation.

Constant Matter Profile $\delta\lambda = \lambda_c$	Periodic Matter Profile $\delta\lambda = A\sin(kx + \phi)$
$\frac{\sin 2\theta_{\mathrm{m}}}{2}\lambda_c e^{i\cos 2\theta_{\mathrm{m}}\lambda_c x}$	$\frac{A\sin 2\theta_{\mathrm{m}}}{4}\sum_{n=-\infty}^{\infty} e^{in\phi}\left(-i^n\right)\frac{2n+1}{z_k}J_n(z_k)e^{i(nk-\omega_{\mathrm{m}})x}$

Table 3.4: Comparison of the off diagonal element of Hamiltonian for constant matter density profile and the periodic matter density profile.

As for Jacobi-Anger expansion, it expands an oscillating matter profile to infinite constant matter potentials. To see it more clearly, we assume that $\delta\lambda = \lambda_c$ is constant. After the unitary transformation, the effective Hamiltonian is

$$H' = \frac{\sin 2\theta_{\mathrm{m}}}{2}\lambda_c \begin{pmatrix} 0 & e^{2i\eta(x)} \\ e^{-2i\eta(x)} & 0 \end{pmatrix}, \tag{3.93}$$

where $\eta(x) = -\frac{\omega_{\mathrm{m}}}{2}x + \frac{\cos 2\theta_{\mathrm{m}}}{2}\lambda_c x$ and we have chosen $\eta(0) = 0$. The 12 element of the Hamiltonian becomes

$$\frac{\sin 2\theta_{\mathrm{m}}}{2}\lambda_c e^{2i\eta(x)} = \frac{\sin 2\theta_{\mathrm{m}}}{2}\lambda_c e^{2i\left(\frac{\omega_{\mathrm{m}}}{2} + \frac{\cos 2\theta_{\mathrm{m}}}{2}\lambda_c\right)x}. \tag{3.94}$$

The significance of it is to show that a constant matter profile will result in a simple exponential term. However, as we move on to periodic matter profile, we have a Hamiltonian element of the form

$$h = \frac{\sin 2\theta_{\mathrm{m}}}{2}A\sin(kx + \phi)e^{2i\left(-\frac{\omega_{\mathrm{m}}}{2}x + \frac{A\cos 2\theta_{\mathrm{m}}}{2k}\cos(kx+\phi)\right)}, \tag{3.95}$$

as derived in Eqn. 3.52. To compare with the constant matter case, we make a table of relevant terms in Hamiltonian, Table 3.4.

The periodic profile comes into the exponential. Jacobi-Anger expansion (Eqn. **??**) expands the periodic matter profile into infinite constant matter profiles. By comparing the two cases, we conclude that $\cos 2\theta_{\mathrm{m}}\lambda_c$ corresponds to nk. The RWA approximation we used to drop fast oscillatory terms in the summation is to find the most relevant constant matter profile per se.

The big question is which constant matter profiles are the most important ones? Mathematically, we require the phase to be almost zero, i.e. Eqn. 3.61 or

$$n_0 k - \omega_m \sim 0, \tag{3.96}$$

where $n_0 = \text{Round}\left(\frac{\omega_m}{k}\right)$.

We define an effective matter density out of the Jacobi-Anger expanded series

$$\lambda'_c = \frac{n_0 k}{\cos 2\theta_m}. \tag{3.97}$$

Then we can rewrite the RWA requirement as

$$\lambda'_c - \cos 2\theta_m \omega_m = 0. \tag{3.98}$$

The Resonances

Now we check the Hamiltonian again to see if we could locate some physics. In the newly defined basis and using scaled quantities

$$\hat{\mathbf{H}} = \begin{pmatrix} 0 & \hat{h} \\ \hat{h}^* & 0 \end{pmatrix}, \tag{3.99}$$

where

$$\hat{h} = \frac{1}{2}\hat{B}_n e^{i(n\hat{k}-1)\hat{x}}, \tag{3.100}$$

and

$$\hat{B}_n = (-i)^n \hat{k} \tan 2\theta_m n J_n(\frac{\hat{A}}{\hat{k}} \cos 2\theta_m). \tag{3.101}$$

It becomes much more clearer if we plug $\hat{h}$ back into Hamiltonian. What we find is that

$$\hat{\mathbf{H}} = \sum_{n=-\infty}^{\infty} \begin{pmatrix} 0 & -\frac{1}{2}\hat{B}_n e^{i(n\hat{k}-1)\hat{x}} \\ -\frac{1}{2}\hat{B}_n^* e^{-i(n\hat{k}-1)\hat{x}} & 0 \end{pmatrix}. \tag{3.102}$$

With some effort, we find that the solution to the second amplitude of the wave function is

$$\psi_2 = \frac{i}{\hat{B}_n \hat{W}} e^{-i(n\hat{k}-1)\hat{x}} \left|\hat{B}_n\right|^2 \sin\left(\frac{1}{2}(n\hat{k} - 1 - \hat{W})\hat{x}\right),\qquad(3.103)$$

where

$$\hat{W} = \sqrt{(n\hat{k} - 1)^2 + \left|\hat{B}_n\right|^2}.\qquad(3.104)$$

At this stage, it is quite obvious that our system is a composite Rabi oscillation system. For each specific n term we write down the hopping probability from light state to the heavy state,

$$P_{\text{L}\to\text{H}}^{(n)} = \frac{\left|\hat{B}_n\right|^2}{\left|\hat{B}_n\right|^2 + (n\hat{k} - 1)^2} \sin^2\left(\frac{\hat{q}^{(n)}}{2}\hat{x}\right),\qquad(3.105)$$

where

$$\Gamma^{(n)} = \left|\hat{B}_n\right|,\quad \text{width of resonance } (n\hat{k} \text{ as parameter})\qquad(3.106)$$

$$\hat{q}^{(n)} = \sqrt{|\Gamma^{(n)}|^2 + (n\hat{k} - 1)^2},\quad \text{frequency of oscillations}\qquad(3.107)$$

We define the scaled quantities,

$$\hat{x} = \omega_\text{m}x,\qquad(3.108)$$

$$\hat{h} = h/\omega_\text{m},\qquad(3.109)$$

$$\hat{B}_n = B_n/\omega_\text{m},\qquad(3.110)$$

$$\hat{k} = k/\omega_\text{m},\qquad(3.111)$$

$$\hat{A} = A/\omega_\text{m},\qquad(3.112)$$

$$\hat{q} = q/\omega_\text{m}.\qquad(3.113)$$

Just a comment. B_n is used here because I actually want to use it for multi-frequency case and I just think B_n is better than F.

Resonance width of each order of resonance (each n) should be calculated analytically.

To find the exact width is hopeless since we need to inverse Bessel functions. Nonetheless, we can assume that the resonance is very narrow so that $|F|^2$ doesn't change a lot. With the assumption, the FWHM (Full Width at Half Maximum) is found be setting the amplitude to half, which is

$$\Gamma = \left| \frac{\hat{F}}{n_0} \right| = \left| \hat{k} \tan 2\theta_\mathrm{m} \frac{J_{n_0}(n_0 \hat{A} \cos 2\theta_\mathrm{m}/\hat{k})}{n_0} \right|. \tag{3.114}$$

To verify this result, we compare it with the width found numerically from the exact amplitude.

Given this result, and equation 3.69, we infer that the coefficient in front of the phase term of 12 element in Hamiltonian is related to the width, while the the the deviation from the exact resonance is given by $\hat{g} = n_0 \hat{k} - 1$.

the width of the resonance is

$$\Gamma = \left| \frac{F}{n_0} \right|. \tag{3.115}$$

3.6.2 Multiple Matter Density Frequencies

However, as we proceed to the more realistic matter profile, multi-frequency matter profiles are necessary. Generally, we choose the perturbation matter profile upon a constant background to be

$$\delta\lambda(x) = \sum_n A_n \sin(k_n x + \phi_n). \tag{3.116}$$

Applying the Rabi basis and solving for η we conclude that

$$\eta(x) = -\frac{\omega_\mathrm{m}}{2} x - \frac{\cos 2\theta_\mathrm{m}}{2} \sum_n \frac{A_n}{k_n} \cos(k_n x + \phi_n). \tag{3.117}$$

We formulate the Hamiltonian in Rabi basis to be the form

$$H^{(R)} = -\frac{1}{2}\sigma_3 + \begin{pmatrix} 0 & h \\ h^* & 0 \end{pmatrix}, \tag{3.118}$$

We write down the off diagonal element h for the multi-frequency matter density profile

$$h = \frac{\sin 2\theta_{\mathrm{m}}}{2} \sum_a A_a \sin(k_a x + \phi_a) e^{-i\omega_{\mathrm{m}} x} \prod_a \sum_{n=-\infty}^{\infty} (-i)^n J_n(z_{k_a}) e^{in(k_a x + \phi_a)} \tag{3.119}$$

To demonstrate the procedure of Jacobi-Anger expansion as well as the technique to decompose the problem into simple Rabi oscillations, we adopt a two frequencies matter density scenario.

To work out the equation of motion that we could solve, we deal with two frequencies first,

$$\delta\lambda(x) = A_1 \sin(k_1 x + \phi_1) + A_2 \sin(k_2 x + \phi_2), \tag{3.120}$$

while

$$h = \frac{\sin 2\theta_{\mathrm{m}}}{2} \sum_{a=1}^{2} A_a \sin(k_a x + \phi_a) e^{-i\omega_{\mathrm{m}} x} \prod_{a=1}^{2} \sum_{n=-\infty}^{\infty} (-i)^n J_n(z_{k_a}) e^{in(k_a x + \phi_a)}. \tag{3.121}$$

A useful trick for multiplication of two summations is

$$\sum_n a_n \sum_{\mathrm{m}} b_{\mathrm{m}} = \sum_{N=-\infty}^{\infty} \sum_{m+n=N} a_n b_{\mathrm{m}} = \sum_{N=-\infty}^{\infty} \sum_{n=-\infty}^{N} a_n b_{N-n}. \tag{3.122}$$

For further simplifications of the problem, we follow a rule to sum over a line $m+n = N$ then sum over N, which is illustrated in Fig. 3.13.
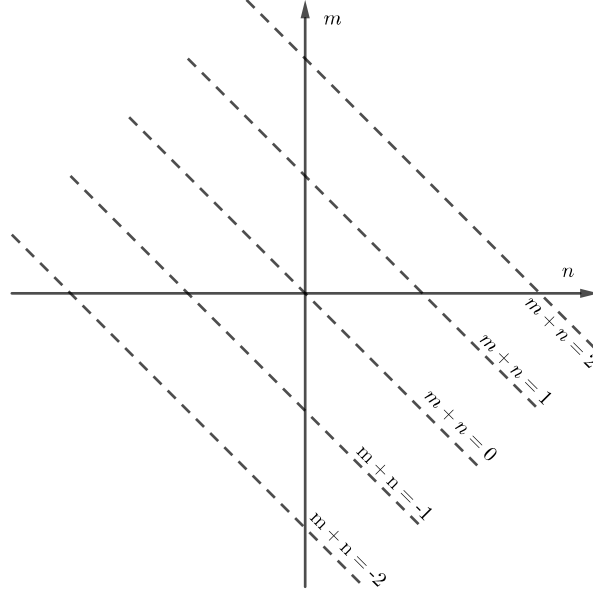
Figure 3.13: Rewrite multiplication of summations into summations only. The horizontal axis is for the summation index n and the vertical axis is for the summation index m. The dashed lines are the lines of equal $m + n$.

The multiplication in Eqn. 3.121 becomes

$$
\begin{aligned}
h = & \frac{\sin 2\theta_\mathrm{m}}{2} \sum_{a=1}^{2} A_a \sin(k_a x + \phi_a) e^{-i\omega_\mathrm{m} x} \\
& \sum_{N=-\infty}^{\infty} \sum_{n=-\infty}^{N} (-i)^n J_n(z_{k_1}) e^{in(k_1 x + \phi_1)} (-i)^{N-n} J_{N-n}(z_{k_2}) e^{i(N-n)(k_2 x + \phi_2)} \\
= & \frac{\sin 2\theta_\mathrm{m}}{2} \sum_{a=1}^{2} A_a \sin(k_a x + \phi_a) e^{-i\omega_\mathrm{m} x} \\
& \sum_{N=-\infty}^{\infty} \sum_{n=-\infty}^{N} (-i)^N J_n(z_{k_1}) J_{N-n}(z_{k_2}) e^{in((k_1 - k_2)x + \phi_1 - \phi_2) + iN(k_2 x + \phi_2)} \quad (3.123)
\end{aligned}
$$

To proceed on, we rewrite $\sum_{a=1}^{2} A_a \sin(k_a x + \phi_a)$,

$$A_1 \sin(k_1 x + \phi_1) + A_2 \sin(k_2 x + \phi_2)$$
$$= \frac{A_1}{2i} \left(e^{i(k_1 x + \phi_1)} + e^{-i(k_1 x + \phi_1)} \right) + \frac{A_2}{2i} \left(e^{i(k_2 x + \phi_2)} + e^{-i(k_2 x + \phi_2)} \right). \tag{3.124}$$

We define

$$h = h_1 + h_2, \tag{3.125}$$

where

$$h_1 = \frac{A_1 \sin 2\theta_{\mathrm{m}}}{4i} \left(\sum_{N=-\infty}^{\infty} \sum_{n=-\infty}^{N} (-i)^N J_n(z_{k_1}) J_{N-n}(z_{k_2}) e^{i((n+1)(k_1 x + \phi_1) + (N-n)(k_2 x + \phi_2) - \omega_{\mathrm{m}} x)} \right.$$
$$\left. \sum_{N=-\infty}^{\infty} \sum_{n=-\infty}^{N} (-i)^N J_n(z_{k_1}) J_{N-n}(z_{k_2}) e^{i((n-1)(k_1 x + \phi_1) + (N-n)(k_2 x + \phi_2) - \omega_{\mathrm{m}} x)} \right), \tag{3.126}$$

and

$$h_2 = \frac{A_2 \sin 2\theta_{\mathrm{m}}}{4i} \left(\sum_{N=-\infty}^{\infty} \sum_{n=-\infty}^{N} (-i)^N J_n(z_{k_1}) J_{N-n}(z_{k_2}) e^{i(n(k_1 x + \phi_1) + (N-n+1)(k_2 x + \phi_2) - \omega_{\mathrm{m}} x)} \right.$$
$$\left. \sum_{N=-\infty}^{\infty} \sum_{n=-\infty}^{N} (-i)^N J_n(z_{k_1}) J_{N-n}(z_{k_2}) e^{i(n(k_1 x + \phi_1) + (N-n-1)(k_2 x + \phi_2) - \omega_{\mathrm{m}} x)} \right). \tag{3.127}$$

We keep only terms that are integers for each summation to satisfy the relations

$$(n_{11,N} + 1)k_1 + (N - n_{11,N})k_2 - \omega_{\mathrm{m}} \sim 0 \tag{3.128}$$

$$(n_{12,N} - 1)k_1 + (N - n_{12,N})k_2 - \omega_{\mathrm{m}} \sim 0 \tag{3.129}$$

$$n_{21,N} k_1 + (N - n_{21,N} + 1)k_2 - \omega_{\mathrm{m}} \sim 0 \tag{3.130}$$

$$n_{22,N} k_1 + (N - n_{22,N} - 1)k_2 - \omega_{\mathrm{m}} \sim 0. \tag{3.131}$$

so that the x dependent exponential almost vanishes (obtain the largest wavelength in fact). Notice that each $n_{ij,N}$ depends on the summation index N.

We solve each $n_{ij,N}$,

$$n_{11,N} \sim \text{Round} \left[\frac{\omega_\text{m} - Nk_2 - k_1}{k_1 - k_2} \right] \tag{3.132}$$

$$n_{12,N} \sim \text{Round} \left[\frac{\omega_\text{m} - Nk_2 + k_1}{k_1 - k_2} \right] \tag{3.133}$$

$$n_{21,N} \sim \text{Round} \left[\frac{\omega_\text{m} - (N+1)k_2}{k_1 - k_2} \right] \tag{3.134}$$

$$n_{22,N} \sim \text{Round} \left[\frac{\omega_\text{m} - (N-1)k_2}{k_1 - k_2} \right]. \tag{3.135}$$

Another important constrain is that $n \leq N$, thus we have

$$N_{11} \sim \text{Round} \left[\frac{\omega_\text{m} - k_1}{k_1} \right] \tag{3.136}$$

$$N_{12} \sim \text{Round} \left[\frac{\omega_\text{m} + k_1}{k_1} \right] \tag{3.137}$$

$$N_{21} \sim \text{Round} \left[\frac{\omega_\text{m} - k_2}{k_1} \right] \tag{3.138}$$

$$N_{22} \sim \text{Round} \left[\frac{\omega_\text{m} + k_2}{k_1} \right], \tag{3.139}$$

for each summation over N and we require $N \geq N_{ij}$ for each summation. We also assumed $k_1 > k_2$. In other words, N_{ij} are the lower limits of the summations over N's.

We keep only the resonance terms for the summation over n's,

$$h_1 \approx \frac{A_1 \sin 2\theta_\text{m}}{4i} \left(\sum_{N=N_{11}}^{\infty} (-i)^N J_{n_{11}}(z_{k_1}) J_{N-n_{11}}(z_{k_2}) e^{i((n_{11}+1)(k_1 x + \phi_1) + (N-n_{11})(k_2 x + \phi_2) - \omega_\text{m} x)} \right.$$

$$\left. \sum_{N=N_{12}}^{\infty} (-i)^N J_{n_{12}}(z_{k_1}) J_{N-n_{12}}(z_{k_2}) e^{i((n_{12}-1)(k_1 x + \phi_1) + (N-n_{12})(k_2 x + \phi_2) - \omega_\text{m} x)} \right), \tag{3.140}$$

and

$$h_2 \approx \frac{A_2 \sin 2\theta_\text{m}}{4i} \left(\sum_{N=N_{21}}^{\infty} (-i)^N J_{n_{21}}(z_{k_1}) J_{N-n_{21}}(z_{k_2}) e^{i(n_{21}(k_1 x + \phi_1) + (N-n_{21}+1)(k_2 x + \phi_2) - \omega_\text{m} x)} \right.$$

$$\left. \sum_{N=N_{22}}^{\infty} (-i)^N J_{n_{22}}(z_{k_1}) J_{N-n_{22}}(z_{k_2}) e^{i(n_{22}(k_1 x + \phi_1) + (N-n_{22}-1)(k_2 x + \phi_2) - \omega_\text{m} x)} \right). \tag{3.141}$$

One can imagine how hard it is to solve the equation of motion with this h. More approximations are required. We will use the approximations that Kelly Patton et al used [21].

By looking at the Hamiltonian, we can identify terms like this

$$h_a = \left(\frac{\sin 2\theta_{\mathrm{m}}}{2} A_a \sin(k_a x + \phi_a) e^{-i\omega_{\mathrm{m}} x} \sum_{n=-\infty}^{\infty} (-i)^n J_n(z_{k_a}) e^{in(k_a x + \phi_a)} \right)$$
$$\prod_{b \neq a} \sum_{n=-\infty}^{\infty} (-i)^n J_n(z_{k_b}) e^{in(k_b x + \phi_b)}, \tag{3.142}$$

where the parenthesis part is what we would have if only one frequency is used and we also have

$$h = \sum_a h_a, \tag{3.143}$$

for all frequencies. This reminds us that each of these terms means the interference due to other frequencies. As a simple example, we demonstrate two-frequency case.

The two-frequency matter perturbation system has a Hamiltonian element H_{12}

$$h = h_1 + h_2, \tag{3.144}$$

where

$$h_1 = -\frac{k_1 \tan 2\theta_{\mathrm{m}}}{2} \sum_{n_1=-\infty}^{\infty} (-i)^{n_1} n_1 J_{n_1}(z_{k_1}) e^{i(n_1 k_1 - \omega_{\mathrm{m}})x} e^{in_1 \phi_1}$$
$$\sum_{n_2=-\infty}^{\infty} (-i)^{n_2} J_{n_2}(z_{k_2}) e^{i(n_2 k_2)x} e^{in_2 \phi_2}, \tag{3.145}$$

$$h_2 = -\frac{k_2 \tan 2\theta_{\mathrm{m}}}{2} \sum_{n_2=-\infty}^{\infty} (-i)^{n_2} n_2 J_{n_2}(z_{k_2}) e^{i(n_2 k_2 - \omega_{\mathrm{m}})x} e^{in_2 \phi_2}$$
$$\sum_{n_1=-\infty}^{\infty} (-i)^{n_1} J_{n_1}(z_{k_1}) e^{in_1 k_1 x} e^{in_1 \phi_1} \tag{3.146}$$

with red color coding the second frequency and blue coding the first frequency. h is symmetric under exchange of index 1, 2 since the exchange simply switches h_1 and h_2.

The next question to ask is which term dominates. To grasp a clue, we need to identify which term in the summation dominates. Without a good analytical analysis, the only way to do is to numerically calculate the effect of each order.

By order, we are already thinking of a dominating term which is not true. Nonetheless, we assume RWA can be applied to the part that looks like one frequency only. In our two-frequency example, first RWA leads to

$$
h_1 \approx -\frac{k_1 \tan 2\theta_{\mathrm{m}}}{2}(-i)^{n_{1,0}} n_{1,0} J_{n_{1,0}}(z_{k_1}) e^{i(n_{1,0}k_1 - \omega_{\mathrm{m}})x} e^{in_{1,0}\phi_1}
$$
$$
\sum_{n_2=-\infty}^{\infty} (-i)^{n_2} J_{n_2}(z_{k_2}) e^{i(n_2 k_2)x} e^{in_2\phi_2}, \tag{3.147}
$$

$$
h_2 \approx -\frac{k_2 \tan 2\theta_{\mathrm{m}}}{2}(-i)^{n_{2,0}} n_{2,0} J_{n_{2,0}}(z_{k_2}) e^{i(n_{2,0}k_2 - \omega_{\mathrm{m}})x} e^{in_{2,0}\phi_2}
$$
$$
\sum_{n_1=-\infty}^{\infty} (-i)^{n_1} J_{n_1}(z_{k_1}) e^{in_1 k_1 x} e^{in_1\phi_1}, \tag{3.148}
$$

where

$$
n_{1,0} = \mathrm{Round}\left[\frac{\omega_{\mathrm{m}}}{k_1}\right], \tag{3.149}
$$

$$
n_{2,0} = \mathrm{Round}\left[\frac{\omega_{\mathrm{m}}}{k_2}\right]. \tag{3.150}
$$

With this approximation, we can use RWA again by requiring

$$
(n_{1,0}k_1 - \omega_{\mathrm{m}} + n_2 k_2)x \sim 0, \tag{3.151}
$$

$$
(n_1 k_1 - \omega_{\mathrm{m}} + n_{2,0}k_2)x \sim 0, \tag{3.152}
$$

where the integer solutions are

$$
n'_{2,0} = \mathrm{Round}\left[\frac{n_{1,0}k_1 - \omega_{\mathrm{m}}}{k_2}\right], \tag{3.153}
$$

$$
n'_{1,0} = \mathrm{Round}\left[\frac{n_{2,0}k_1 - \omega_{\mathrm{m}}}{k_1}\right]. \tag{3.154}
$$

Now we can remove all the summations using another RWA approximation. However, whether it holds is up to investigation.

The final result is

$$
\begin{aligned}
h_1 &\approx -\frac{k_1 \tan 2\theta_{\mathrm{m}}}{2}(-i)^{n_{1,0}} n_{1,0} J_{n_{1,0}}(z_{k_1}) e^{i(n_{1,0}k_1-\omega_{\mathrm{m}})x} e^{in_{1,0}\phi_1}(-i)^{n'_{2,0}} J_{n'_{2,0}}(z_{k_2}) e^{i(n'_{2,0}k_2)x} e^{in'_{2,0}\phi_2} \\
&= -\frac{k_1 \tan 2\theta_{\mathrm{m}}}{2}(-i)^{n_{1,0}+n'_{2,0}} e^{i(n_{1,0}\phi_1+n'_{2,0}\phi_2)} n_{1,0} \\
&\quad J_{n_{1,0}}(z_{k_1}) J_{n'_{2,0}}(z_{k_2}) e^{i(n_{1,0}k_1-\omega_{\mathrm{m}}+n'_{2,0}k_2)x} \\
&\equiv \frac{F_1}{2} e^{i(n_{1,0}k_1-\omega_{\mathrm{m}}+n'_{2,0}k_2)x},
\end{aligned}
\tag{3.155, 3.156}
$$

$$
\begin{aligned}
h_2 &\approx -\frac{k_2 \tan 2\theta_{\mathrm{m}}}{2}(-i)^{n_{2,0}} n_{2,0} J_{n_{2,0}}(z_{k_2}) e^{i(n_{2,0}k_2-\omega_{\mathrm{m}})x} e^{in_{2,0}\phi_2} \sum_{n_1=-\infty}^{\infty} (-i)^{n_1} J_{n_1}(z_{k_1}) e^{in_1 k_1 x} e^{in_1\phi_1} \\
&= -\frac{k_2 \tan 2\theta_{\mathrm{m}}}{2}(-i)^{n_{2,0}+n'_{1,0}} e^{i(n_{2,0}\phi_2+n'_{1,0}\phi_1)} n_{2,0} \\
&\quad J_{n_{2,0}}(z_{k_2}) J_{n'_{1,0}}(z_{k_1}) e^{i(n_{2,0}k_2-\omega_{\mathrm{m}}+n'_{1,0}k_1)x} \\
&\equiv \frac{F_2}{2} e^{i(n_{2,0}k_2-\omega_{\mathrm{m}}+n'_{1,0}k_1)x}.
\end{aligned}
\tag{3.157, 3.158}
$$

Lowest order only works for very special cases where on of the wave vectors is very close to resonance. To fix this problem, we could add more higher orders, however, what does it mean to have higher orders needs a discussion.

We will develop a protocol to decide which order to include. The first thought of higher orders is to add more from the summation before the last RWA. However, it is highly suspicious that this is just like the one frequency case which has a very fast drop in the resonance width as we go to higher orders. This guess needs proof, numerically and analytically. When we mentioned higher orders, we actually mean higher orders in both n_1 and n_2. Notice that we can always write the 12 element of

Hamiltonian as Eqn. 3.163, i.e.,

$$h = h_1 + h_2 \tag{3.159}$$

$$= \sum_{n_1=-\infty}^{\infty} \sum_{n_2=-\infty}^{\infty} B_{n_1,n_2}(k_1, k_2) \Phi e^{i(n_1 k_1 + n_2 k_2 - \omega_{\mathrm{m}})x}$$

$$+ \sum_{n_1=-\infty}^{\infty} \sum_{n_2=-\infty}^{\infty} B_{n_2,n_1}(k_2, k_1) \Phi e^{i(n_1 k_1 + n_2 k_2 - \omega_{\mathrm{m}})x}$$

$$= \sum_{n_1=-\infty}^{\infty} \sum_{n_2=-\infty}^{\infty} \left(B_{n_1,n_2}(k_1, k_2) + B_{n_2,n_1}(k_2, k_1) \right) \Phi e^{i(n_1 k_1 + n_2 k_2 - \omega_{\mathrm{m}})x}, \tag{3.160}$$

without any approximations.

- One of the choices of adding higher orders is to use $n_1 = \mathrm{Round}\left[\frac{\omega_{\mathrm{m}}}{k_1}\right]$ and $n_2 = \mathrm{Round}\left[\frac{n_1 k_1 - \omega_{\mathrm{m}}}{k_2}\right]$ as the lowest order in h_1 and $n_2 = \mathrm{Round}\left[\frac{\omega_{\mathrm{m}}}{k_2}\right]$ and $n_1 = \mathrm{Round}\left[\frac{n_2 k_2 - \omega_{\mathrm{m}}}{k_1}\right]$ as the lowest order in h_2. Adding higher orders means we add or remove one from n_1 in h_1 and recalculate n_2, while add or remove one from n_2 in h_2 and recalculate n_1.

  That is to say, we always keep the RWA condition for the last RWA process. What can be changed is the first assumption that the most important term is when only one frequency is relevant which is not always true.

  As an example, we now consider $n_{i,\pm 1} = n_{i,0} \pm 1$ and $n'_{i,\pm 1} = \mathrm{Round}\left[\frac{n_{j,\pm 1} k_j - \omega_{\mathrm{m}}}{k_i}\right]$ with $j \neq i$, thus we replace $n_{i,0}$ with $n_{i,\pm 1}$ to get higher order corrections, c.f. Fig. 3.14.

  In realistic physical systems, it is more likely to have a matter profile so that we have the bottom left situation. In other words, RWA method breaks down in the most interesting case.

- Another choice is to add or remove one for both n_1 and n_2 for both terms in the Hamiltonian. The approach will define the order n_{order} first, as will be applied to the n's. As an example, adding first order to n_1 will include all
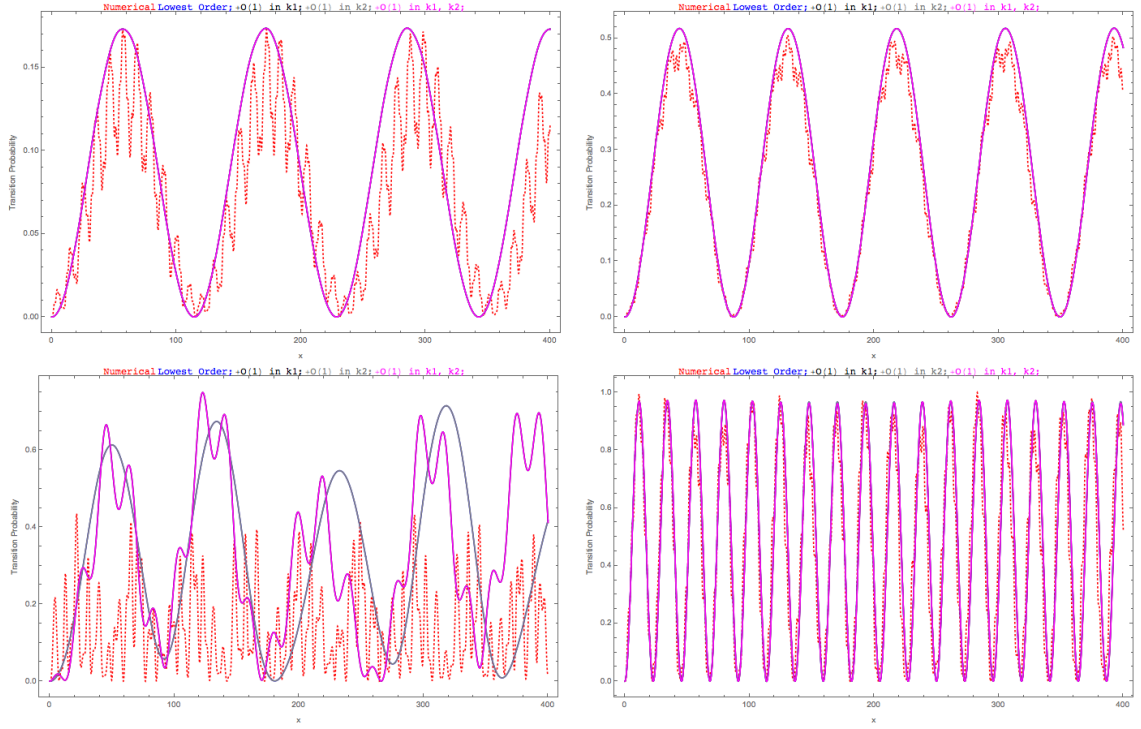
Figure 3.14: Top Left: Smaller wavenumber $k_1 = 0.95$ is at resonance and it has smaller perturbation amplitude ($k_2 = 1.55$); Top Right: Smaller wavenumber $k_1 = 0.95$ is at resonance and it has larger perturbation amplitude ($k_2 = 1.55$); Bottom Left: Larger wavenumber $k_2 = 0.95$ is at resonance and it has smaller perturbation amplitude ($k_1 = 0.35$); Bottom Right: Larger wavenumber $k_2 = 0.95$ is at resonance and it has larger perturbation amplitude ($k_1 = 0.35$). Red dotted line is numerical solution, black line is lowest approximation of k_2, magenta is higher order approximation of k_2.

the possible combinations of $n_1, n_1 \pm 1$ for both terms without changing n_2. As an example, we compare the different orders of n_1 only with the numerical calculation without approximations in Fig. 3.15.

- Now according to the complete expression of the $_{12}$ element of Hamiltonian Eqn. 3.163, there is no difference between n_1 and n_2. Thus whenever we talk about different orders, we should not distinguish between the two integers. However, how to define zero order is not clear to me at this point. To find
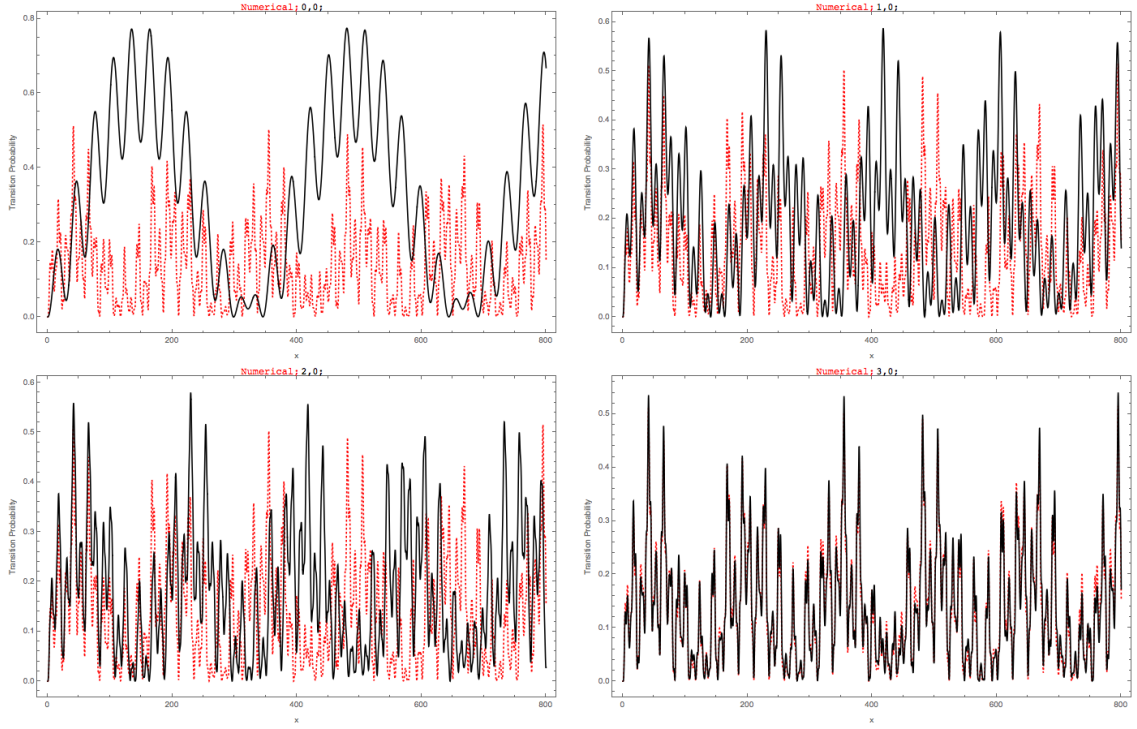
Figure 3.15: Compare the different orders with the numerical calculation without approximations, where red dotted line is the numerical calculation without approximation. As we could see from the figure, including up to third order in n_1 fixes the deviation from numerical calculation (red dotted line). The wave vectors are $k_1 = 0.5$, $k_2 = 0.8$, amplitudes are $A_1 = 0.1k_1^{-5/3}$, $A_2 = 0.1k_2^{-5/3}$, mixing angle in background matter is $\theta_\mathrm{m} = \pi/5$.

out, we need to know the resonance width of each pair of integers. The insight comes from the single frequency result. The width for single frequency $\Gamma = \left| \frac{\hat{F}}{n_0} \right| = \left| \hat{k} \tan 2\theta_\mathrm{m} \frac{J_{n_0}(n_0 \hat{A} \cos 2\theta_\mathrm{m}/\hat{k})}{n_0} \right|$. depends on the coefficient in front of the phase in the Hamiltonian and the integer. The task is to derive or guess the resonance width for each pair of integers n_1, n_2.

As for a more systematic treatment of the two-frequency case, we geometrize the problem. The 12 element can be written as

$$h = h_1 + h_2, \tag{3.161}$$

where

$$h_1 = \sum_{n_1=-\infty}^{\infty} \sum_{n_2=-\infty}^{\infty} \left(-(-i)^{n_1+n_2} \frac{\tan 2\theta_m}{2} n_1 k_1 J_{n_1}(z_{k_1}) J_{n_2}(z_{k_2}) \right) e^{i(n_1\phi_1+n_2\phi_2)} e^{i(n_1k_1+n_2k_2-\omega_m)x},$$

$$h_2 = \sum_{n_1=-\infty}^{\infty} \sum_{n_2=-\infty}^{\infty} \left(-(-i)^{n_1+n_2} \frac{\tan 2\theta_m}{2} n_2 k_2 J_{n_1}(z_{k_1}) J_{n_2}(z_{k_2}) \right) e^{i(n_1\phi_1+n_2\phi_2)} e^{i(n_1k_1+n_2k_2-\omega_m)x}.$$

For simplicity, we define

$$B_{n_1,n_2}(k_1, k_2, A_1, A_2) = -(-i)^{n_1+n_2} \tan 2\theta_m n_1 k_1 J_{n_1}(z_{k_1}) J_{n_2}(z_{k_2})$$

$$= -(-i)^{n_1+n_2} \tan 2\theta_m n_1 k_1 J_{n_1}(\frac{A_1}{k_1} \cos 2\theta_m) J_{n_2}(\frac{A_2}{k_2} \cos 2\theta_m),$$

$$\Phi = e^{i(n_1\phi_1+n_2\phi_2)}.$$

Notice that

$$B_{n_2,n_1}(k_2, k_1, A_2, A_1) = -(-i)^{n_1+n_2} \tan 2\theta_m n_2 k_2 J_{n_1}(\frac{A_1}{k_1} \cos 2\theta_m) J_{n_2}(\frac{A_2}{k_2} \cos 2\theta_m).$$

Using these definitions, we rewrite the Hamiltonian 12 element

$$h = h_1 + h_2 \tag{3.162}$$

$$= \frac{1}{2} \sum_{n_1=-\infty}^{\infty} \sum_{n_2=-\infty}^{\infty} B_{n_1,n_2}(k_1, k_2, A_1, A_2) \Phi e^{i(n_1k_1+n_2k_2-\omega_m)x}$$

$$+ \frac{1}{2} \sum_{n_1=-\infty}^{\infty} \sum_{n_2=-\infty}^{\infty} B_{n_2,n_1}(k_2, k_1, A_2, A_1) \Phi e^{i(n_1k_1+n_2k_2-\omega_m)x}$$

$$= \frac{1}{2} \sum_{n_1=-\infty}^{\infty} \sum_{n_2=-\infty}^{\infty} \left(B_{n_1,n_2}(k_1, k_2, A_1, A_2) + B_{n_2,n_1}(k_2, k_1, A_2, A_1) \right) \Phi e^{i(n_1k_1+n_2k_2-\omega_m)x}$$

$$= \frac{1}{2} \sum_{n_1=-\infty}^{\infty} \sum_{n_2=-\infty}^{\infty} B_2 n_1, n_2(k_1, k_2, A_1, A_2) \Phi e^{i(n_1k_1+n_2k_2-\omega_m)x}, \tag{3.163}$$

where $B_2 n_1, n_2(k_1, k_2, A_1, A_2) \equiv B_{n_1,n_2}(k_1, k_2, A_1, A_2) + B_{n_2,n_1}(k_2, k_1, A_2, A_1)$ is what we are interested in.

Comparing this expression with the single frequency one which is almost the same structure if we remove the two sums, and using the result 3.92, we can infer that the

transition probability,

$$P_{1\to2}(x) = \frac{|\hat{B}_2|^2}{|\hat{B}_2|^2 + \hat{g}_2^2} \sin^2\left(\frac{q_2}{2}x\right), \tag{3.164}$$

where $\hat{B}_2 = \frac{B_2}{\omega_{\mathrm{m}}} = \frac{B_{n_1,n_2}(k_1,k_2,A_1,A_2)+B_{n_2,n_1}(k_2,k_1,A_2,A_1)}{\omega_{\mathrm{m}}}$ and $\hat{g}_2 = \frac{g}{\omega_{\mathrm{m}}} = n_1\hat{k}_1 + n_2\hat{k}_2 - 1$ which tells us how far from resonance and $q_2 = \sqrt{|\hat{B}_2|^2 + \hat{g}^2}$.

The width then is similar to 3.115, except that we could not define the width as a function of single variables since two wave vector are used. However, it is still reasonable to give the FWHM condition,

$$n_1\hat{k}_1 + n_2\hat{k}_2 - 1 = \pm|\hat{B}_2| = \left|\frac{B_{n_1,n_2}(k_1,k_2,A_1,A_2) + B_{n_2,n_1}(k_2,k_1,A_2,A_1)}{\omega_{\mathrm{m}}}\right|. \tag{3.165}$$

For a given pair of integers n_1, n_2, we could find the amplitude as a function of k_1, k_2.

A solution shows that this is correct. The solution to the second element of wave function is

$$\psi_{b2} = i\frac{|\hat{B}_2|^2 e^{-\frac{i}{2}\hat{g}_2\hat{x}}}{\hat{B}_2\sqrt{|\hat{B}_2|^2 + \hat{g}^2}} \sin\left(\frac{\sqrt{|\hat{B}_2|^2 + \hat{g}^2}}{2}x\right). \tag{3.166}$$

It is very confusing when we write down the requirement for width 3.165, since we need to assume $|\hat{F}_2|$ to be almost constant to arrive this result. What values of $\hat{k}_1, \hat{k}_2$ do we need to calculate $|\hat{F}_2|$? The idea is to find the FWHM (Full Width Half Maximum) when a point is deviating from the line. To be specific, we find the line that is the resonance using $n_1k_1 + n_2k_2 = 1$, which is plotted as dashed red line in 3.16. To characterize the distance, we need a line that is perpendicular to this red dashed resonance line, which also is passing through the values of $(k_10, k_2) = (k_{10}, k_{20})$ which is given in the system. Under this scheme, the resonance width is define as the distance from the resonance line when the amplitude reduces to half on this blue dotted perpendicular line.

In the language of algebra, we could derive the interception point of the two lines,
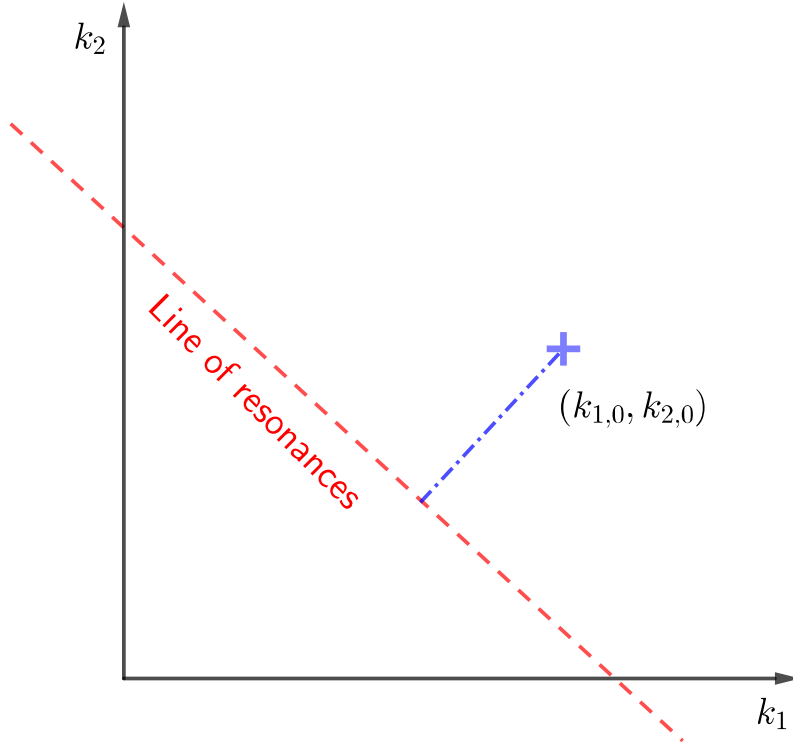
Figure 3.16: Diagram of Width for two frequencies in matter density profile. The red dashed line is the line when the resonances happen. The cross is the location for a system that with two frequencies in density profile, $k_{1,0}$ and $k_{2,0}$. The blue dash dotted line indicates the distance between the actual frequencies of the system and the resonances.

which is

$$k_{1,\text{intercept}} = \frac{n_2^2 k_{10} + n_2 k_{20} + n_1}{n_1^2 + n_2^2}, \qquad (3.167)$$

$$k_{2,\text{intercept}} = \frac{n_1}{n_2} k_{1,\text{intercept}} - \frac{1}{n_2}, \qquad (3.168)$$

where k_{10} and k_{20} are the values given in the matter perturbation of the system.

Using this method, we can define a reasonable width for two frequency matter

perturbation case,

$$\Gamma_2 = \frac{B_2(k_{1,\text{intercept}}, k_{2,\text{intercept}})}{\sqrt{n_1^2 + n_2^2}}. \tag{3.169}$$

To apply the width in a problem, we need to calculate the distance between the given point (k_{10}, k_{20}) of the system to a certain resonance line which depends on $n_1, n_2, A_1, A_2, \theta_m$. This is as simple as point to line distance, which is calculated using

$$d = \frac{|n_1 k_{10} + n_2 k_{20} - 1|}{\sqrt{n_1^2 + n_2^2}}. \tag{3.170}$$

The requirement for a pair of (n_1, n_2) to be important is determined by defining a quantity that compares the distance from a certain resonance line with the width of this resonance line,

$$Q_2 = \frac{d}{\Gamma_2}. \tag{3.171}$$

3.7 Conclusions

The solar neutrinos behave very differently from lab experiments since the Sun provides a high matter density lab which can not be built on the Earth. What's even more exotic, in a supernova explosion, 10^{58} neutrinos are released from the proto-neutron star, which is of radius 10km, in a few seconds. The huge number density of neutrinos and large density of matter both change the neutrino oscillations dramatically. The matter effect in supernova is also much more complicated than MSW for solar neutrinos since the rich distribution of matter density and high speed motion. In addition to matter effect, neutrino neutrino interaction will be very efficient because of the high neutrino number density.

Apart from the emission of neutrinos from nuclear reactions of electron capture and positron emission in the solar interior, supernova environment also gives rise

to Bremsstrahlung pair neutrino production, electron-positron neutrino pair production, which brings all three flavors and also anti-neutrinos into the spectra. However, even the with the presence of intensive interaction between neutrinos and the leptons and hardrons, which thermalize the neutrinos in the supernova core, the neutrino spectrum escaping from the supernova core is not completely Fermi-Dirac distribution. Nonetheless, it is possible to parametrize it using nominal Fermi-Dirac distribution,[11]

$$f(E) \propto \frac{E^2}{1 + \exp(E/kT - \mu)}. \tag{3.172}$$

Some numerical results show that there is a deviation from this Fermi-Dirac distribution [7, 10]. Meanwhile, Keil Mathias and Georg Raffelt showed that it is good enough to approximate the neutrino spectrum from supernova in Monte Carlo simulations using the so called "alpha fit",

$$f(E) \propto E^\alpha \exp\left(-(\alpha + 1)\frac{E}{\langle E \rangle}\right), \tag{3.173}$$

where $\langle E \rangle$ is the average energy, or the first moment of energy. The values from Monte Carlo simulations falls into the range $\alpha = 2.5 \sim 5$, which clearly shows the spectra are pinched. It's a hint that the detection of deviation from nominal Fermi-Dirac distribution will show evidence of core-collapse information.

Even though we understand solar neutrinos well, the neutrino oscillations of supernova explosions are not so to our complete knowledge. The flavor content is subject to the solution to the neutrino oscillations. Phenomena such as spectral split due to neutrino-neutrino interaction and matter effect reshape the neutrino spectra significantly. That being said, more research on supernova neutrinos, especially supernova neutrino oscillations is critical to understand supernova explosion mechanisms, as well as future observation of supernova neutrino data.

In conclusion, we have provided an interpretation for neutrino flavor conversion in fluctuating matter with the help of Rabi oscillations. The work provided two different points of view that is related to Rabi oscillations.

The first point of view was to interpret the neutrino flavor conversions in background matter basis. In this basis, matter density fluctuations will introduced a fluctuation part to the diagonal elements of the Hamiltonian, which means that the energy gap is fluctuating if we draw analogy between this Hamiltonian and the Hamiltonian of Rabi oscillations. For neutrino flavor conversions in a single frequency matter profile, the neutrino flavor oscillations becomes large when the matter fluctuation frequency is close to the energy gap, which is the resonance condition. We anticipated that the fluctuations of energy gap have limited effects on neutrino flavor conversions under this resonance condition. Thus the matter fluctuation only works as a pure flipping field that converts neutrinos from one flavor to another.

As we added more frequencies of matter density fluctuations, the neutrino flavor conversions becomes nontrivial due to the interferences between the difference matter profile frequencies. To quantify the interference between different Rabi oscillation modes, we defined relative detuning which describes how off-resonance a Rabi oscillation is. In the case of single frequency Rabi oscillations, the relative detuning becomes 0 under the resonance condition. As a second frequency is added to the oscillations, the energy gap is shifted due to this new frequency. A measure of the interference effect is to consider the relative detuning of the first frequency which is at resonance, under the shifted energy gap. Numerical results verified this conjecture. With the interference mechanism, we revisit the single frequency matter profile neutrino oscillations.

Another view is to switch to a basis where the neutrino oscillations Hamiltonian is decomposed into infinite Rabi oscillations. Equivalently speaking, the oscillations are consequences of superposition of Rabi oscillations, which we call modes of oscillations. This view was applied to emphasis the approximations that the change of energy gap due to matter fluctuation can be neglected under resonance condition in the previous background matter basis.

Bibliography

[1]   C L Cowan et al. "Detection of the Free Neutrino: a Confirmation." In: *Science (New York, N.Y.)* 124.3212 (July 1956), pp. 103–4.

[2]   B Pontecorvo. "Neutrino experiments and the problem of conservation of leptonic charge". In: *Sov. Phys. JETP* 26.5 (1968), pp. 984–988.

[3]   J.N. Bahcall. "The solar neutrino problem". In: *Nuclear Instruments and Methods* 110 (July 1973), pp. 381–384.

[4]   L. Wolfenstein. "Neutrino oscillations in matter". In: *Physical Review D* 17.9 (May 1978), pp. 2369–2374.

[5]   P.I. Krastev and A.Yu. Smirnov. "Parametric effects in neutrino oscillations". In: *Physics Letters B* 226.3-4 (Aug. 1989), pp. 341–346.

[6]   F. N. Loreti and A. B. Balantekin. "Neutrino oscillations in noisy media". In: *Physical Review D* 50.8 (Oct. 1994), pp. 4762–4770. arXiv: 9406003 [nucl-th].

[7]   T. Totani et al. "Future Detection of Supernova Neutrino Burst and Explosion Mechanism". In: *The Astrophysical Journal* 496.1 (Mar. 1998), pp. 216–225.

[8]   E. Kh Akhmedov. "Parametric resonance in neutrino oscillations in matter". In: *Pramana* 54.1 (Jan. 2000), pp. 47–63. arXiv: 9907435 [hep-ph].

[9]   Michael F Altmann, Rudolf L Mößbauer, and Lothar J N Oberauer. "Solar neutrinos". In: *Reports on Progress in Physics* 64.1 (Jan. 2001), pp. 97–146.

[10]   Mathias Th. Keil. "Supernova Neutrino Spectra and Applications to Flavor Oscillations". PhD thesis. 2003. arXiv: `0308228 [astro-ph]`.

[11]   Georg G. Raffelt et al. "Supernova neutrinos: Flavor-dependent fluxes and spectra". In: *Neutrino oscillations and their origin. Proceedings, 4th International Workshop, NOON2003, Kanazawa, Japan, February 10-14, 2003.* 2003, pp. 380–387. arXiv: `astro-ph/0303226 [astro-ph]`.

[12]   Huaiyu Duan, George M. Fuller, and Yong-Zhong Qian. "Analysis of collective neutrino flavor transformation in supernovae". In: *Physical Review D* 74.12 (Dec. 2006), p. 123004. arXiv: `0703776 [astro-ph]`.

[13]   Huaiyu Duan, George M. Fuller, and Yong-Zhong Qian. "Collective neutrino flavor transformation in supernovae". In: *Physical Review D* 74.12 (Dec. 2006), p. 123004. arXiv: `0703776 [astro-ph]`.

[14]   Alexander Friedland and Andrei Gruzinov. "Neutrino signatures of supernova turbulence". July 2006.

[15]   J. P. Kneller and G. C. McLaughlin. "Monte Carlo neutrino oscillations". In: *Physical Review D* 73.5 (Mar. 2006), p. 056003.

[16]   R. W. Boyd. *Nonlinear Optics.* Third. Elsevier, 2008. ISBN: 978-0-12-369470-6.

[17]   I. Ploumistakis, S.D. Moustaizis, and I. Tsohantjis. "Towards laser based improved experimental schemes for multiphoton pair production from vacuum". In: *Physics Letters A* 373.32 (2009), pp. 2897–2900.

[18]   James Kneller and Cristina Volpe. "Turbulence effects on supernova neutrinos". In: *Physical Review D* 82.12 (Dec. 2010), p. 123004. arXiv: `1006.0913`.

[19]   Eg Adelberger and a Garćıa. "Solar fusion cross sections. II. The pp chain and CNO cycles". In: *Reviews of Modern …* 83.March (2011). arXiv: `arXiv: 1004.2318v3`.

[20] James P. Kneller, Gail C. McLaughlin, and Kelly M. Patton. "Stimulated neutrino transformation with sinusoidal density profiles". In: *Journal of Physics G: Nuclear and Particle Physics* 40.5 (May 2013), p. 055002. arXiv: `arXiv:1202.0776v1`.

[21] Kelly M. Patton, James P. Kneller, and Gail C. McLaughlin. "Stimulated neutrino transformation through turbulence". In: *Physical Review D* 89.7 (Apr. 2014), p. 073022. arXiv: `arXiv:1407.7835v1`.

[22] Sean M. Couch and Christian D. Ott. "The Role of Turbulence in Neutrino-driven Core-collapse Supernova Explosions". In: *The Astrophysical Journal* 799.1 (Jan. 2015), p. 5.

[23] B. Muller and H.- T. Janka. "Non-radial instabilities and progenitor asphericities in core-collapse supernovae". In: *Monthly Notices of the Royal Astronomical Society* 448.3 (Feb. 2015), pp. 2141–2174.

[24] Hans-Thomas Janka, Tobias Melson, and Alexander Summa. "Physics of Core-Collapse Supernovae in Three Dimensions: A Sneak Preview". In: *Annual Review of Nuclear and Particle Science* 66.1 (2016), pp. 341–375. arXiv: `1602.05576`.

[25] C. Patrignani et al. "Review of Particle Physics". In: *Chin. Phys.* C40.10 (2016), p. 100001.

[26] Hans-Thomas Janka. *Neutrino Emission from Supernovae*. Ed. by Athem W. Alsabti and Paul Murdin. Cham: Springer International Publishing, 2017, pp. 1575–1604. ISBN: 978-3-319-21846-5.

[27] E. Kemp. "The Deep Underground Neutrino Experiment: The precision era of neutrino physics". In: *Astronomische Nachrichten* 338.9-10 (2017), pp. 993–999.